Cell

Mitocytosis, a migrasome-mediated mitochondrial quality-control process

Graphical abstract

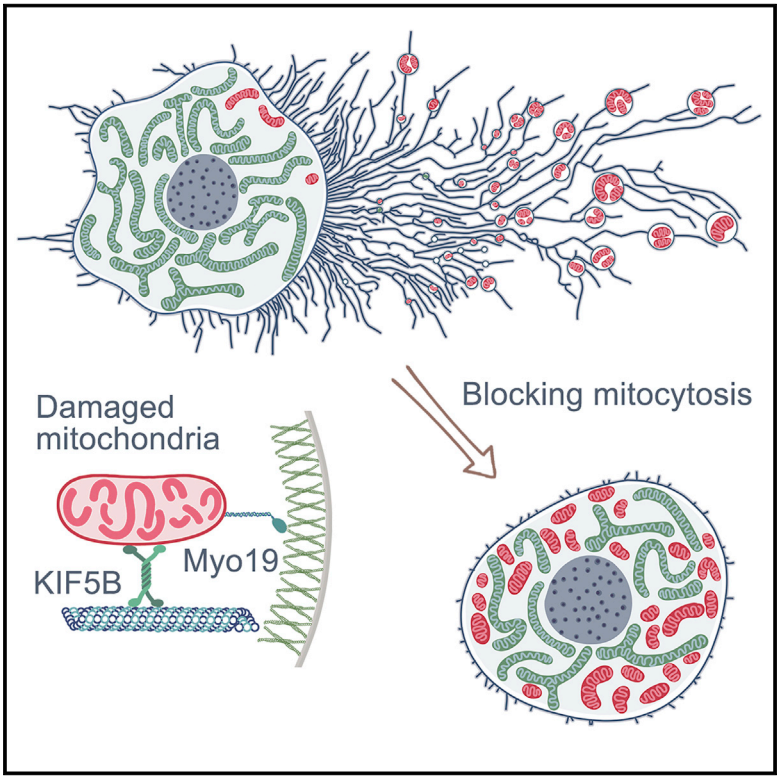

Highlights

- Mild mitochondrial stress triggers disposal of damaged mitochondria by migrasomes
- In this process (mitocytosis), motor proteins selectively bind damaged mitochondria
- Damaged mitochondria become localized at the cell periphery to facilitate mitocytosis
- Mitocytosis maintains mitochondrial quality and viability in neutrophils *in vivo*

Authors

Haifeng Jiao, Dong Jiang, Xiaoyu Hu, ..., Yau-Huei Wei, Xiaoyu Hu, Li Yu

Correspondence

liyulab@mail.tsinghua.edu.cn

In brief

Migrating cells selectively remove damaged mitochondria to maintain homeostasis in a process called mitocytosis.

Jiao et al., 2021, Cell *184*, 2896–2910
May 27, 2021
https://doi.org/10.1016/j.cell.2021.04.027

CellPress

CellPress

Cell

Article

Mitocytosis, a migrasome-mediated mitochondrial quality-control process

Haifeng Jiao,[1,4] Dong Jiang,[1,4] Xiaoyu Hu,[1] Wanqing Du,[1] Liangliang Ji,[2] Yuzhuo Yang,[2] Xiaopeng Li,[1] Takami Sho,[1] Xuan Wang,[1] Ying Li,[1] Yu-Ting Wu,[3] Yau-Huei Wei,[3] Xiaoyu Hu,[2] and Li Yu[1,5,*]

[1]State Key Laboratory of Membrane Biology, Tsinghua University-Peking University Joint Centre for Life Sciences, Beijing Frontier Research Center for Biological Structure, School of Life Sciences, Tsinghua University, Beijing 100084, China

[2]Institute for Immunology and School of Medicine, Tsinghua University, Beijing 100084, China

[3]Center for Mitochondrial Medicine and Free Radical Research, Changhua Christian Hospital, Changhua City, Taiwan 50046

[4]These authors contributed equally

[5]Lead contact

*Correspondence: liyulab@mail.tsinghua.edu.cn

https://doi.org/10.1016/j.cell.2021.04.027

SUMMARY

Damaged mitochondria need to be cleared to maintain the quality of the mitochondrial pool. Here, we report mitocytosis, a migrasome-mediated mitochondrial quality-control process. We found that, upon exposure to mild mitochondrial stresses, damaged mitochondria are transported into migrasomes and subsequently disposed of from migrating cells. Mechanistically, mitocytosis requires positioning of damaged mitochondria at the cell periphery, which occurs because damaged mitochondria avoid binding to inward motor proteins. Functionally, mitocytosis plays an important role in maintaining mitochondrial quality. Enhanced mitocytosis protects cells from mitochondrial stressor-induced loss of mitochondrial membrane potential (MMP) and mitochondrial respiration; conversely, blocking mitocytosis causes loss of MMP and mitochondrial respiration under normal conditions. Physiologically, we demonstrate that mitocytosis is required for maintaining MMP and viability in neutrophils *in vivo*. We propose that mitocytosis is an important mitochondrial quality-control process in migrating cells, which couples mitochondrial homeostasis with cell migration.

INTRODUCTION

As vital organelles for eukaryotic cells, mitochondria are subject to tight quality control (Youle, 2019). Various mechanisms, including mitochondrial proteases, proteasome-mediated degradation of outer mitochondrial membrane (OMM) proteins, degradation of mitochondrial-derived vesicles (MDVs), and mitophagy have been shown play important roles in mitochondrial quality control (Pickles et al., 2018). Most of the known mechanisms to remove damaged mitochondria are based on protease- or proteasome-mediated degradation of mitochondria or mitochondrial proteins. Mitochondria can be shed from cells through various mechanisms (Davis et al., 2014; Hayakawa et al., 2016; Melentijevic et al., 2017; Torralba et al., 2016). Shedding of mitochondria can contribute to mitochondrial quality control (Melentijevic et al., 2017) or serve as a mechanism to mediate horizontal transfer of mitochondria between cells (Hayakawa et al., 2016; Torralba et al., 2016).

Migrasomes are organelles in migrating cells (Ma et al., 2015). During cell migration, retraction fibers are pulled from the rear end of cells, and large vesicular structures named migrasomes grow on the retraction fibers. When the cell migrates away, the retraction fibers break and migrasomes are left behind. Cellular contents such as vesicles and cytosol can be released from the cell through migrasomes. Migrasome formation depends on migration. Blocking migration using the Myosin II inhibitor blebbistatin, or by modulating cell adhesion, inhibits migrasome formation (Wu et al., 2017).

Members of the tetraspanin family have emerged as key regulators of migrasome formation. A subset of tetraspanins, including TSPAN4 and TSPAN9, can induce migrasome formation when overexpressed. Conversely, knocking out the most highly expressed migrasome-forming tetraspanins impairs migrasome formation. Migrasome formation is mediated by assembly of tetraspanin-enriched macrodomains, which increase the bending rigidity of the migrasomal membrane and promote migrasome formation through a biophysical process that we named as the membrane stiffening model (Huang et al., 2019).

Recently, migrasomes have been shown to play a key role in zebrafish organogenesis (Jiang et al., 2019). During zebrafish embryo development, developmental cues such as chemokines, morphogens, and growth factors are enriched in migrasomes and delivered to spatially restricted locations in the embryo to modulate organogenesis. Thus, migrasomes are organelles for non-autonomous cell-cell communication. Whether migrasomes have autonomous functions is not known.

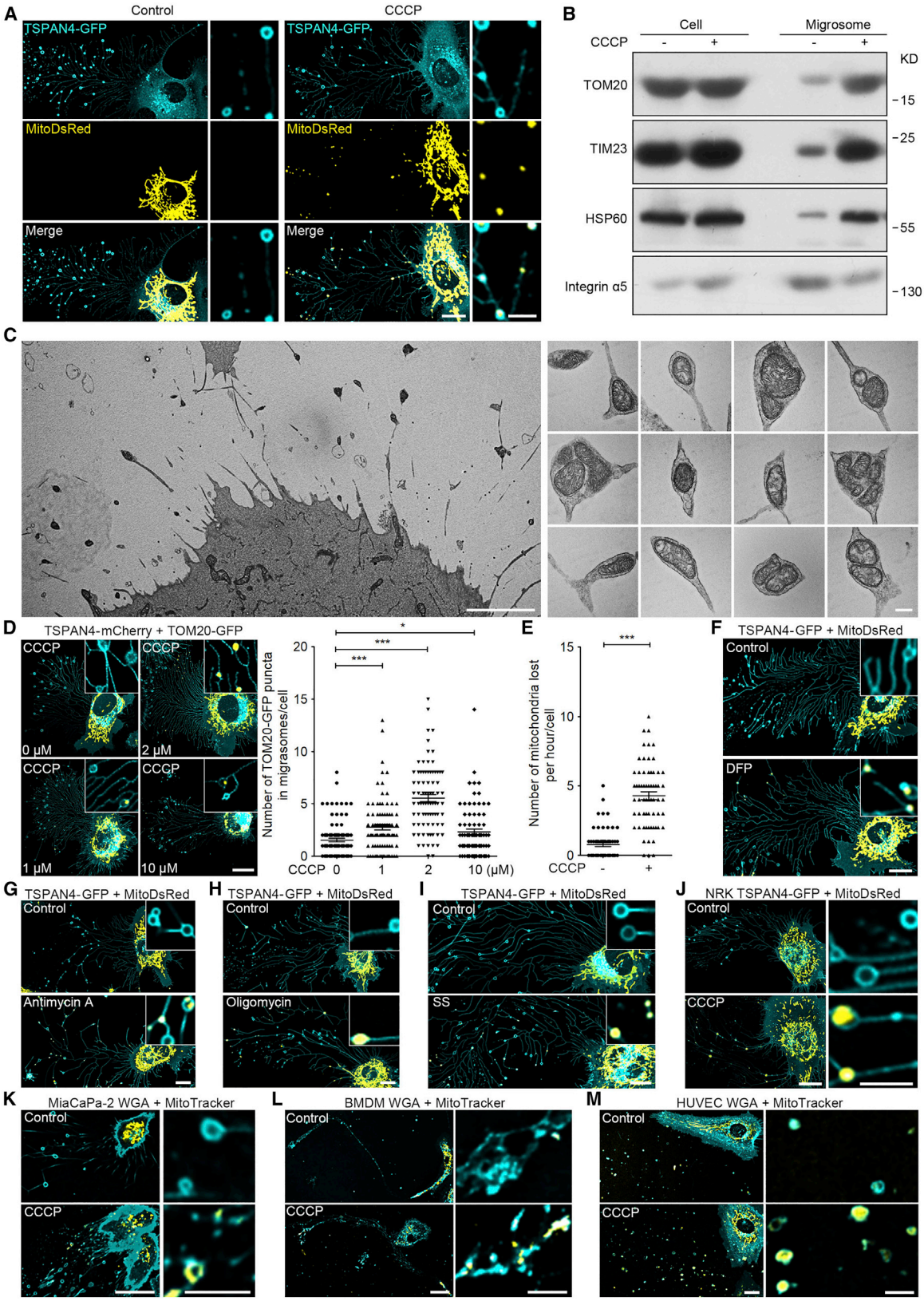

(legend on next page)

RESULTS

Mitochondrial stressors trigger mitocytosis

We started by examining L929 cells expressing TSPAN4-GFP, which labels migrasomes, and MitoDsRed, which labels mitochondria. When we treated the cells with the oxidative phosphorylation uncoupler carbonyl cyanide 3 chlorophenylhydrazone (CCCP, 2 μM), we observed the MitoDsRed signal inside migrasomes (Figure 1A). To verify this observation biochemically, we isolated migrasomes before and after CCCP treatment. We found that proteins from the mitochondrial outer membrane, inner membrane, and matrix do indeed accumulate in migrasomes after CCCP treatment (Figure 1B). Transmission electron microscopy (TEM) analysis revealed that, after CCCP treatment, mitochondria indeed accumulate inside migrasomes. We named these mitochondrion-containing migrasomes as mitosomes. Detailed analysis showed that these mitochondria are small, with an average size of 240 nm. These structures are evidently mitochondria, but not MDVs, as the mitochondrial inner membrane and cristae are clearly visible. The swollen mitochondrial cristae imply that the mitochondria inside migrasomes may have been damaged. A single mitosome can contain multiple mitochondria (Figure 1C). Since migrasomes are eventually left behind the migrating cell, the translocation of mitochondria into migrasomes suggests that mitochondria can be cleared from cells by migrasomes. We named this process as mitocytosis.

We found that as low as 1 μM CCCP is enough to induce mitocytosis. In cells treated with 10 μM CCCP, which is the dose used for inducing mitophagy, mitocytosis is barely induced (Figures 1D). The rate of mitocytosis is modest, with eviction of an average of 4.4 mitochondrial puncta per hour (Figure 1E). Besides CCCP, all the mitochondrial stressors we tested (Deferiprone [DFP], Antimycin A, and Oligomycin) can induce mitocytosis (Figures 1F–1H). In addition, we found that starvation also enhances mitocytosis (Figure 1I). CCCP treatment induced mitocytosis in all the cultured mammalian cells we tested (Figures 1J–1M). These data suggest that mitocytosis is a general mechanism that is activated by various mitochondrial stresses and in a variety of cells.

Mitochondrial positioning and dynamics during mitocytosis

Next, we investigated the molecular mechanism underlying mitocytosis. We found that, during mitocytosis, the highly dynamic tubular mitochondria have extensive outward extensions. Once the tips of tubular mitochondria reach the proximity of the plasma membrane, the tips undergo fission from the mitochondrial network, generating fragments that adhere to areas close to the plasma membrane. Eventually, when the cells migrate away, the ''trapped'' mitochondrial fragments are left on the retraction fibers and subsequently move into migrasomes (Figure 2A; Video S2). In contrast, in the control cells, although mitochondria extend to the plasma membrane, these mitochondria just retract away from the plasma membrane (Video S1).

TEM analysis revealed that the mitochondrial network is segmented into two zones (Figure S1A). In areas close to the bottom of the cell immediately above the plasma membrane, almost all mitochondria have a condensed matrix and swollen cristae, which indicates that these mitochondria are damaged. Some of these damaged mitochondria are localized at the entrance of retraction fibers. Treatment with 2 μM CCCP enhances the number of mitochondria on the bottom of cells. In the middle section of cells (along the y axis), most mitochondria still retain their normal morphology, even in cells treated with 2 μM CCCP (Figures 2B–2D). These data suggest that damaged mitochondria are transported to the bottom of the cell and are eventually left behind the cell by mitocytosis.

KIF5B, Drp1, and Myosin19 are required for mitocytosis

Next, we studied the role of various factors that contribute to mitochondrial dynamics. The outward movement of mitochondria is mediated by KIF5B (Tanaka et al., 1998); we found that KIF5B is required for mitocytosis. In KIF5B knockdown cells, mitocytosis is dramatically reduced (Figure 2E; Figure S2A). Detailed analysis using time-lapse microscopy showed that the outward mobility of mitochondria is markedly reduced in KIF5B-deficient cells (Figure 2H; Video S4). This results in shrinkage of the mitochondrial network to the peri-nuclear region. These data indicate that proximity to the plasma membrane, which is mediated by the outward motor KIF5B, is necessary for mitocytosis.

Next, we investigated the roles of the mitochondrial fusion/fission machinery (Hoppins and Nunnari, 2012; Youle and van der Bliek, 2012). We found that knocking down Drp1, the mitochondrial fission factor, blocks mitocytosis (Figure 2F; Figure S2A). However, knocking down MFN1/MFN2, the

Figure 1. Mitochondrial stressors induce mitocytosis

(A) Confocal image of L929 cells stably expressing TSPAN4-GFP and MitoDsRed (L929-T4G/MR) treated with 2 μM CCCP for 10 h. Scale bar, 20 μm. Right panels, enlarged region of interesting (ROI). Scale bar, 5 μm.

(B) Western blot analysis of the migrasome from (A).

(C) Representative transmission electron microscopy (TEM) images of L929 cell treated with 2 μM CCCP. Scale bar, 5 μm. Right panels, enlarged ROI. Scale bar, 200 nm.

(D) Confocal images of L929 cells stably expressing TSPAN4-mCherry and TOM20-GFP (L929-T4G/T20R) treated with 2 μM CCCP. Scale bar, 20 μm. Right panel, statistical analysis of the number of TOM20-GFP puncta in migrasomes per cell. Error bars, the mean ± SEM n > 100 cells from three independent experiments. Two-tailed unpaired t tests were used for statistical analyses.

(E) Confocal images of L929-T4G/T20R cells treated with 2 μM CCCP. Time-lapse images were acquired at intervals of 125 s. The number of mitochondria lost per hour was quantified and shown as the mean ± SEM for triplicate samples of >50 cells. Two-tailed unpaired t tests were used for statistical analyses.

(F–H) Confocal images of L929-T4G/MR cells treated with indicated reagents for 12 h. Scale bar, 20 μm.

(I) Confocal images of L929-T4G/MR cells cultured in serum-starved (SS) medium for 10 h. Scale bar, 20 μm.

(J) Confocal images of NRK cells stably expressing TSPAN4-GFP and MitoDsRed treated with or without 1 μM CCCP. Scale bar, 20 μm. Right panels, enlarged ROI. Scale bar, 5 μm.

(K–M) MiaCaPa-2 (K), BMDM (L), and HUVEC (M) cells, either untreated or treated with 2 μM CCCP, were stained with WGA and Mitotracker and then visualized. Scale bar, 20 μm. Right panels: enlarged ROI. Scale bar, 5 μm.

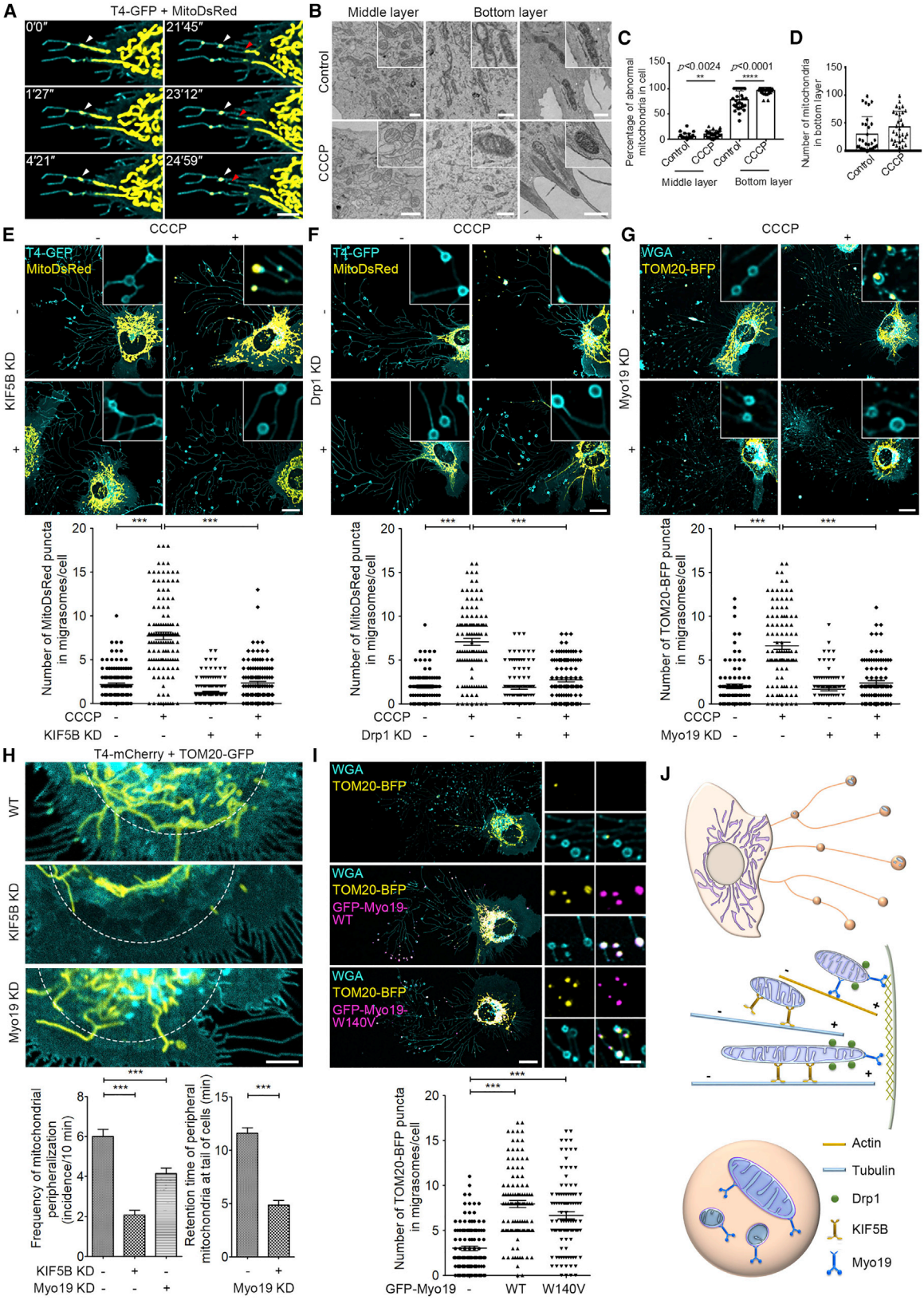

(legend on next page)

mitochondrial fusion factors, only has a marginal effect in promoting mitocytosis (Figures S2A and S2B).

Time-lapse imaging revealed that under CCCP treatment, mitochondria extended into the area close to the plasma membrane and appeared to be trapped in that area (Figure 2H; Video S3). Myosin19 is a mitochondrion-associated myosin that can bind both mitochondria and actin. Myo19 has been shown to mediate the reactive oxygen species (ROS)-induced translocation of mitochondria to filopodia (Shneyer et al., 2017). Moreover, Myo19 has been shown to tether the mitochondria to cortical actin on the plasma membrane (Quintero et al., 2009; Shneyer et al., 2016). As we expected, we found that knockdown of Myo19 blocked mitocytosis (Figure 2G; Figure S2A). In KIF5B knockdown cells, the mitochondrial network shrinks to the peri-nuclear region, and there are very few outward extensions of mitochondria to the plasma membrane (Figure 2H; Video S4). In Myo19 knockdown cells, the extension of mitochondria is only slightly affected (Figure 2H; Video S5). However, the remaining highly dynamic tubular mitochondria that extend to the plasma membrane in Myo19 knockdown cells rarely adhere in the vicinity of the plasma membrane area; they just retract back quickly (Figure 2H; Video S5).

Overexpressing Myo19 is sufficient to promote mitocytosis, overexpression of Myo19-W140V, which lacks mobility but retains its mitochondrial localization and actin-binding activity, can still promote mitocytosis, suggesting that Myo19 may contribute to mitocytosis mainly by tethering mitochondria to the cortical actin network on the plasma membrane (Figure 2I).

Put together, these data suggest that KIF5B mediates mitocytosis by pulling mitochondria to the plasma membrane, where Myo19 tethers mitochondria to cortical actin, which is tightly associated with the plasma membrane. Finally, the tips of tubular mitochondria, which bind to cortical actin, undergo Drp1-mediated fission and are then sent into migrasomes (Figure 2J).

Dynein knockdown promotes mitocytosis in untreated cells

We noticed that knocking down dynein, the inward motor on microtubules (Sheng, 2014), is sufficient to trigger mitocytosis in cells that are not exposed to mitochondrial stressors (Figure S2C). Mitocytosis triggered by dynein knockdown can be blocked by knocking down KIF5B, Drp1, or Myo19 (Figures S2D–S2F). This suggests that mitocytosis triggered by dynein knockdown is regulated by the same pathway as mitochondrial stressor-induced mitocytosis.

Mitocytosis disposes of mitochondria with low mitochondrial membrane potential and high ROS

TEM images reveal that the majority of mitochondria inside migrasomes have a condensed matrix and swollen cristae, which suggests that these mitochondria may be damaged (Figure 3A). To directly test this hypothesis, we stained cells with MitoSOX, a dye that labels mitochondria with high ROS, a sign of damaged mitochondria. Indeed, the vast majority of mitochondria inside migrasomes are MitoSOX positive (Figure 3B). Similarly, most mitochondria in migrasomes are TMRM negative, which suggests that the mitochondria in migrasomes have lost their membrane potential (Figure 3C).

Next, we asked whether mitochondria lost their mitochondrial membrane potential (MMP) before or after mitocytosis. When we treated cells with CCCP and then stained them with TMRM, we found that the majority of mitochondria localized at the entrance of retraction fibers are TMRM negative (Figure S3A). This suggests that mitochondria lose their MMP before they are translocated into migrasomes. Similarly, when we treated cells with Antimycin A, we found the majority of mitochondria at the entrance of retraction fibers are MitoSOX positive (Figure S3B), which suggests that mitochondrial damage occurs prior to mitocytosis. Our TEM analysis showed that damaged mitochondria are enriched on the bottom of cells. To characterize the

Figure 2. Mitochondrial positioning and dynamics during mitocytosis

(A) Time-lapse imaging of mitocytosis. L929-T4G/MR cells were treated with 2 μM CCCP. Time-lapse images were acquired at intervals of 87 s. White arrows, the "trapped" mode. Red arrows indicate small mitochondrial fragments moving into migrasomes. Scale bar, 5 μm.

(B) TEM images of L929 cells treated with 2 μM CCCP. Scale bar, 1 μm. Inserts, enlarged ROI.

(C) Quantification of abnormal mitochondria in the middle and bottom layers of L929 cells treated with 2 μM CCCP. Error bars, the mean ± SEM n = 30 cells from three independent experiments. Two-tailed unpaired t tests were used for statistical analyses.

(D) Quantification of the number of mitochondria in the bottom layer of control and CCCP-treated. n = 30 cells from three independent experiments.

(E) L929-T4G/MR cells were infected with nonspecific (NS) or KIF5B-shRNA lentiviral constructs. Cells were treated with 2 μM CCCP for 10 h and then visualized. Scale bar, 20 μm. Bottom panel, statistical analysis of the number of MitoDsRed puncta in migrasomes per cell. Error bars, the mean ± SEM n > 100 cells from three independent experiments. Two-tailed unpaired t tests were used for statistical analyses.

(F) L929-T4G/MR cells were infected with NS or Drp1-shRNA lentiviruses. Cells were treated with 2 μM CCCP and then visualized. Scale bar, 20 μm. Bottom panel, statistical analysis of the number of MitoDsRed puncta in migrasomes per cell. Error bars, the mean ± SEM n > 100 cells from three independent experiments. Two-tailed unpaired t tests were used for statistical analyses.

(G) TOM20-BFP-expressing L929 cells infected with lentivirus bearing indicated shRNAs were treated with 2 μM CCCP and stained with WGA for visualization. Scale bar, 20 μm. Quantification of the number of TOM20-BFP puncta in migrasomes per cell is shown as the mean ± SEM for triplicate samples of >100 cells. Two-tailed unpaired t tests were used for statistical analyses for statistical analyses (bottom panel).

(H) L929-T4G/T20R cells were infected with lentivirus bearing indicated shRNAs. Cells were then treated with 2 μM CCCP and subjected to time-lapse imaging. White dashed lines, the boundary between the peripheral and perinuclear regions. Scale bar, 5 μm. The frequency of mitochondrial peripheralization and the retention time of peripheral mitochondria at the tail of cells were quantified. Error bars, mean ± SEM n = 30 cells from three independent experiments. Two-tailed unpaired t tests were used for statistical analyses. 50 peripheral mitochondria per group were examined.

(I) L929-TOM20-BFP cells stably expressing the indicated forms of Myo19 were stained with WGA for visualization. Scale bar, 20 μm. Right panels, enlarged ROI. Scale bar, 5 μm. Bottom panel, statistical analysis of the number of TOM20-BFP puncta in migrasomes per cell. Error bars, mean ± SEM n > 100 cells from three independent experiments. Two-tailed unpaired t tests were used for statistical analyses.

(J) Schematic diagram of molecular mechanism of mitocytosis.

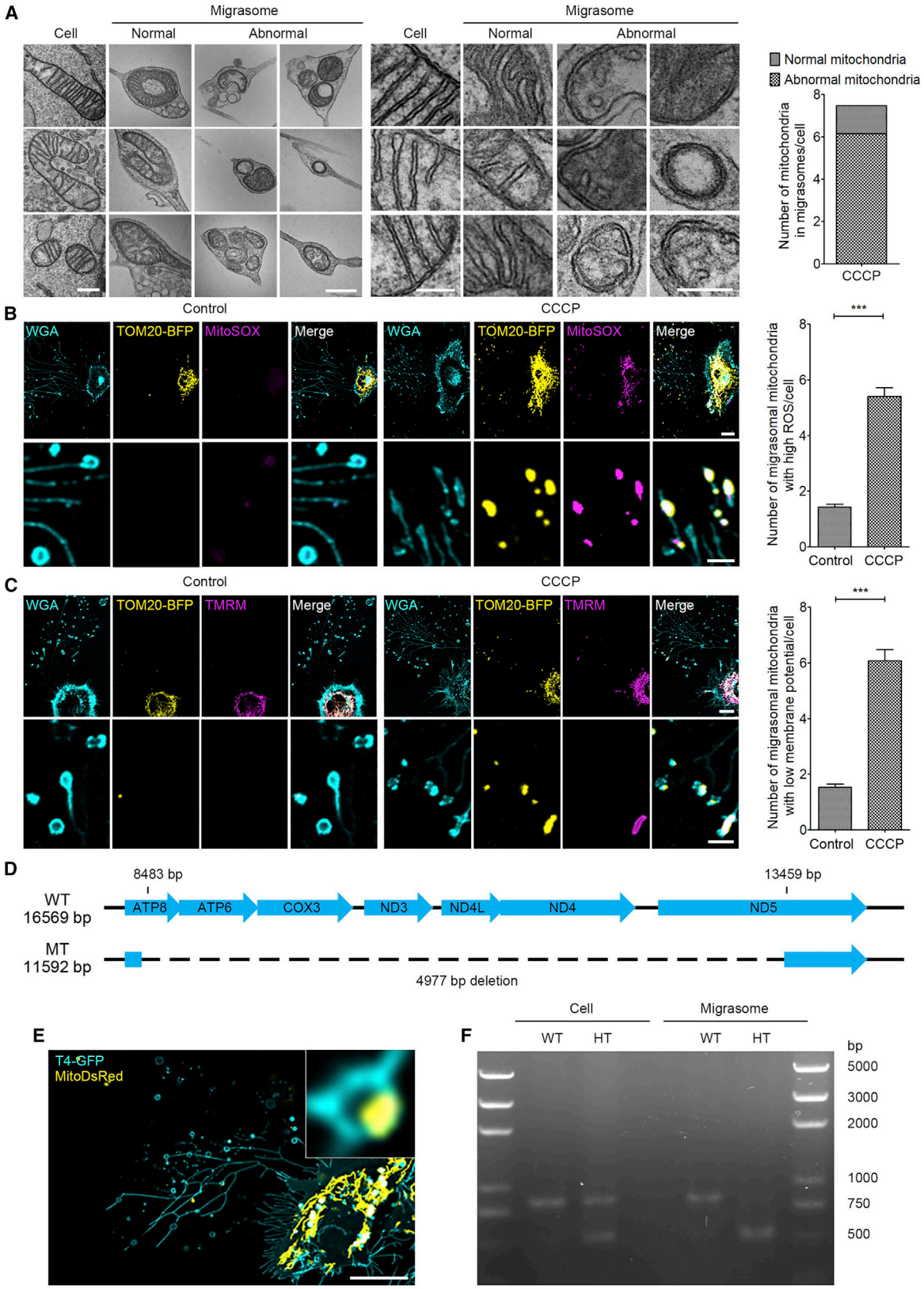

(legend on next page)

properties of mitochondria in different regions of the cell, we carried out 3D confocal imaging analysis of cells, focusing on the bottom, middle, and top planes. We found indeed that the majority of mitochondria in the bottom of cells had lost their MMP after CCCP treatment, while, in the middle section, the majority of mitochondria still have normal MMP (Figure S3D). Similarly, the Mito-SOX signal is also much higher in mitochondria in the bottom layer of cells treated with Antimycin A compared to the middle section (Figure S3C). These data suggest that loss of MMP and generation of ROS occur prior to mitocytosis (Figure S3E).

Mitocytosis selectively disposes of mitochondria with deleterious mutation in mtDNA

If mitocytosis can expel damaged mitochondria, we reasoned that mitochondria with a deleterious mutation in mtDNA should be selectively disposed of by mitocytosis. We tested this hypothesis using a cell model of mitochondrial heteroplasmy (Liu et al., 2009; Porteous et al., 1998; Wei et al., 2001). In this model, both wild-type (WT) mitochondria and mitochondria harboring mutant mtDNA with a 4,977 bp deletion of electron transport chain (ETC) genes are present (Figure 3D). We found that mitochondria harboring mutant mtDNA is selectively enriched in migrasomes (Figures 3E and 3F), which suggests that mitochondria with deleterious mtDNA mutations are selectively disposed of by mitocytosis.

Damaged mitochondria recruit less dynein

How the damaged mitochondria are sensed and transported into migrasomes? TEM analysis revealed that damaged mitochondria may be selectively transported to the cell periphery (Figure 2B). To test this hypothesis, we first analyzed the recruitment of KIF5B and dynein onto isolated mitochondria. We found that treatment of cells with 10 μM CCCP dramatically decreased the mitochondrial recruitment of dynein and increased the recruitment of KIF5B. In contrast, treating cells with 2 μM CCCP only slightly decreased the recruitment of dynein onto mitochondria, while there was no detectable effect on the recruitment of KIF5B (Figure 4A). The small effect on KIF5B and dynein recruitment to mitochondria in cells treated with 2 μM CCCP is not surprising, because, at this dose, only a very small fraction of mitochondria is damaged.

We devised an *in vitro* assay to further verify this observation. In this assay, the mitochondria isolated from control cells or cells treated with 10 μM CCCP were incubated with the S-100 cytosol fraction isolated from an untreated cell line stably expressing GFP-tagged KIF5B and mCherry-tagged DYNLL1. After incubation, the mitochondria were washed and analyzed for recruitment of the exogenous tagged proteins (Figure 4B). We found that indeed the mitochondria from the CCCP-treated cells had a significantly reduced ability to recruit dynein, while their ability to recruit KIF5B was dramatically enhanced (Figure 4C).

To directly test whether damaged mitochondria are disassociated from dynein and selectively recruit KIF5B, we carried out a modified *in vitro* binding assay that allows us to distinguish between the normal and damaged mitochondria. In this assay, mitochondria are damaged by treating cells with 2 μM CCCP, and the isolated mitochondria are then subjected to fluorescence-activated cell sorting (FACS) based on the low or high MMP and used in the binding assay as described above (Figures 4D and 4E). We found that both the high TMRM and low TMRM populations of mitochondria can recruit a similar level of KIF5B (Figure 4F). This indicates that the enhanced KIF5B recruitment to mitochondria in 10 μM CCCP-treated cells (Figure 4C) results from the global increase of KIF5B recruitment to mitochondria. However, we found that recruitment of dynein is significantly reduced in the low TMRM population (Figure 4F), which suggests that damaged mitochondria do tend to bind less dynein.

These data suggest that, in CCCP-treated cells, damaged mitochondria signal their status and subsequently move to the cell periphery through their intrinsic avoidance of binding dynein, the inward motor, and through globally enhanced KIF5B recruitment to mitochondria.

Mitocytosis protects cells from mitochondrial stress

We reasoned that if mitocytosis can dispose of damaged mitochondria, it may serve as a mitochondrial quality control mechanism to protect mitochondria during stress. To test this hypothesis, we generated cell lines in which either migrasome formation or mitochondrial translocation to migrasomes is enhanced. To enhance migrasome formation, we overexpressed TSPAN4 or TSPAN9, as we previously demonstrated that overexpressing these tetraspanins significantly enhances migrasome formation. To elevate the translocation of mitochondria into migrasomes, we knocked down dynein, which results in enhanced translocation of mitochondria into migrasomes. We found that overexpressing TSPAN4 or TSPAN9, or knocking down dynein, markedly protected cells from CCCP-induced loss of MMP (Figures 5A). To test whether

Figure 3. Mitocytosis disposes of damaged mitochondria

(A) TEM images of 2 μM CCCP treated L929 cells. Scale bar, 500 nm. Middle panel, enlarged ROI. Scale bar, 200 nm. Right panel, the morphological categorization of mitochondria in migrasomes. n = 30 cells from three independent experiments.

(B) Mitochondrial ROS production was analyzed by MitoSOX staining. Scale bar, 20 μm. Bottom panels, enlarged ROI. Scale bar, 5 μm. Right panel, quantification of the number of migrasomal mitochondria with high ROS per cell. n > 100 cells from three independent experiments. Two-tailed unpaired t tests were used for statistical analyses.

(C) Migrasomal mitochondrial membrane potential (MMP) of CCCP treated cells revealed by TMRM staining. Scale bar, 20 μm. Bottom panels: enlarged ROI. Scale bar, 5 μm. The number of migrasomal mitochondria with low MMP per cell was quantified. n > 100 cells from three independent experiments. Two-tailed unpaired t tests (right panel).

(D) Schematic representation of the structure of wild-type (WT) and mutant (MT) mitochondrial DNA.

(E) Confocal images of heteroplasmic (HT) cells stably expressing TSPAN4-GFP and MitoDsRed. Scale bar, 20 μm.

(F) Migrasomes were isolated from wild-type (WT) and heteroplasmic (HT) cells. Purified mtDNA from migrasomes and cell bodies was analyzed by PCR. Top band, WT mtDNA; bottom band, mutant mtDNA. 3 repeats were performed.

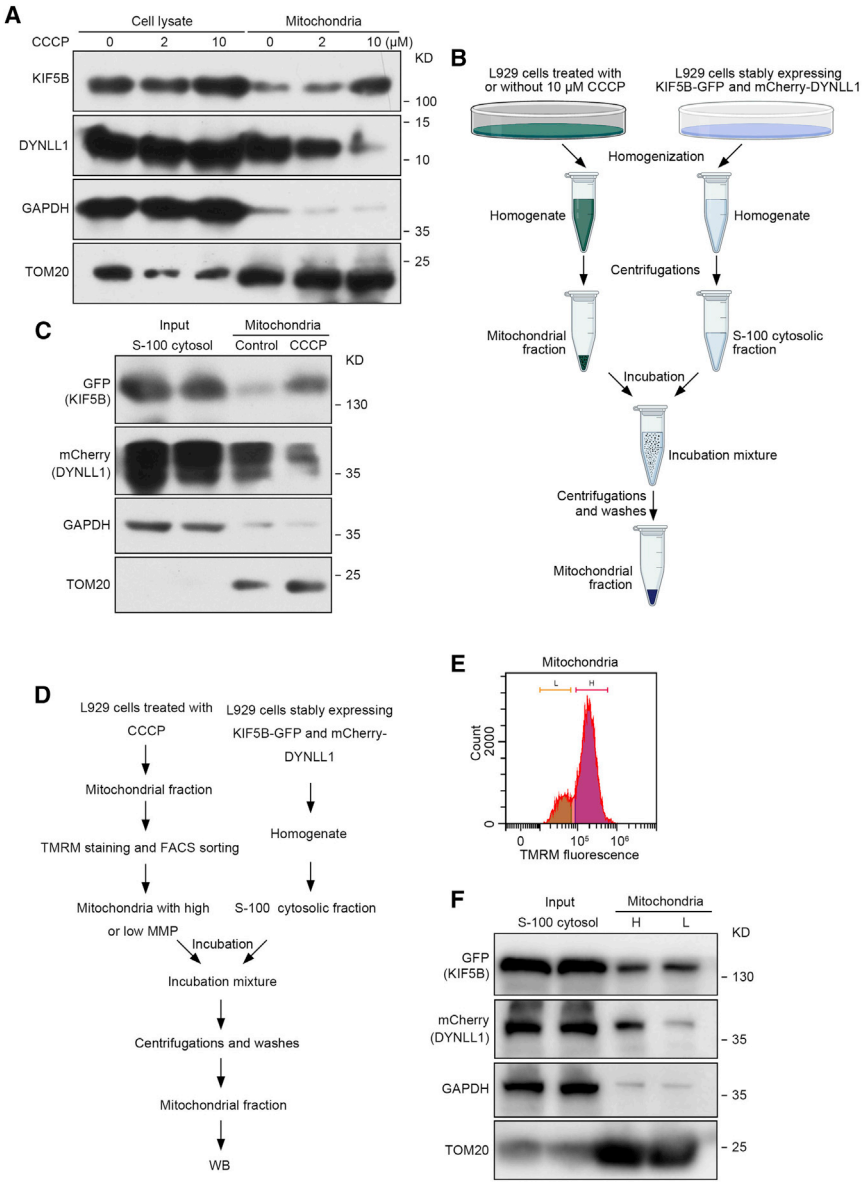

Figure 4. Damaged mitochondria recruit less dynein

(A) Western blot analysis of purified mitochondrial fractions from cells treated with the indicated concentrations of CCCP.

(B) Schematic depiction of the mitochondrial pull-down assay.

(C) Purified mitochondria purified were incubated in S-100 cytosol separated from untreated L929 cells stably expressing KIF5B-GFP and mCherry-DYNLL1 (L929-K5G/DmC) and analyzed by western blotting.

(D–F) Purified mitochondria from CCCP treated cells were stained with TMRM followed by FACS, MMP (L), or MMP (H) were sorted out, incubated in S-100 cytosol from L929-K5G/DmC cells, and then analyzed by western blotting.

this protective effect is indeed due to mitocytosis, we knocked down KIF5B in TSPAN4- or TSPAN9-overexpressing cells and in dynein knockdown cells. We found that KIF5B knockdown abolished the protective effect of tetraspanin overexpression and dynein knockdown (Figure 5B). This suggests that the protective effect of these manipulations is due to mitocytosis.

We reasoned that tetraspanin overexpression or dynein knockdown protected cells from CCCP-induced loss of MMP by enhancing mitocytosis over time, and therefore we should see enhanced recovery of MMP in these cells after acute CCCP treatment. To test this hypothesis, we first treated control, TSPAN4-expressing and dynein knockdown cells with CCCP for 1 h and then cultured them in normal medium for an additional 9 h. We found that, after 1 h of CCCP treatment, all the cells have similar MMP. However, after culture for 9 h in normal medium, the TSPAN4-expressing cells and the dynein knockdown cells have higher MMP than after 1 h of CCCP treatment, while, in control cells, the recovery is much weaker. This result suggests that mitocytosis promotes recovery of MMP over time (Figures S4A–S4C).

We also tested the spare respiration capacity of mitochondria by seahorse analysis. We found that overexpression of TSPAN4 or TSPAN9, or knockdown of dynein, preserved the spare respiration capacity after CCCP treatment (Figure 5C). Finally, we used the MtKeima assay to assess the mitophagy level as a proxy for mitochondrial damage. We found that 2 μm CCCP treatment induces a weak mitophagy signal, which can be reduced by enhanced mitocytosis. In contrast, 10 μM CCCP induces a strong mitophagy signal, which cannot be reduced by enhanced mitocytosis (Figure S4D). These data are consistent with the notion that mitocytosis can mitigate mitochondrial damage induced by mild mitochondrial stress.

Mitocytosis maintains mitochondrial homeostasis

Mitochondrial respiration is coupled with generation of ROS, which can cause mitochondrial damage. We speculated that mitocytosis may play a role in maintaining mitochondrial quality in cells that are not exposed to mitochondrial stressors. To test this hypothesis, we blocked the translocation of mitochondria into migrasomes by knocking down KIF5B. We also blocked migrasome formation by inhibiting cell migration. We found that both treatments markedly reduced the MMP (Figure 5D). Conversely, overexpression of TSPAN4 or TSPAN9, or knockdown of dynein, significantly elevated the MMP (Figure 5E). Blocking mitocytosis also reduces the spare respiration

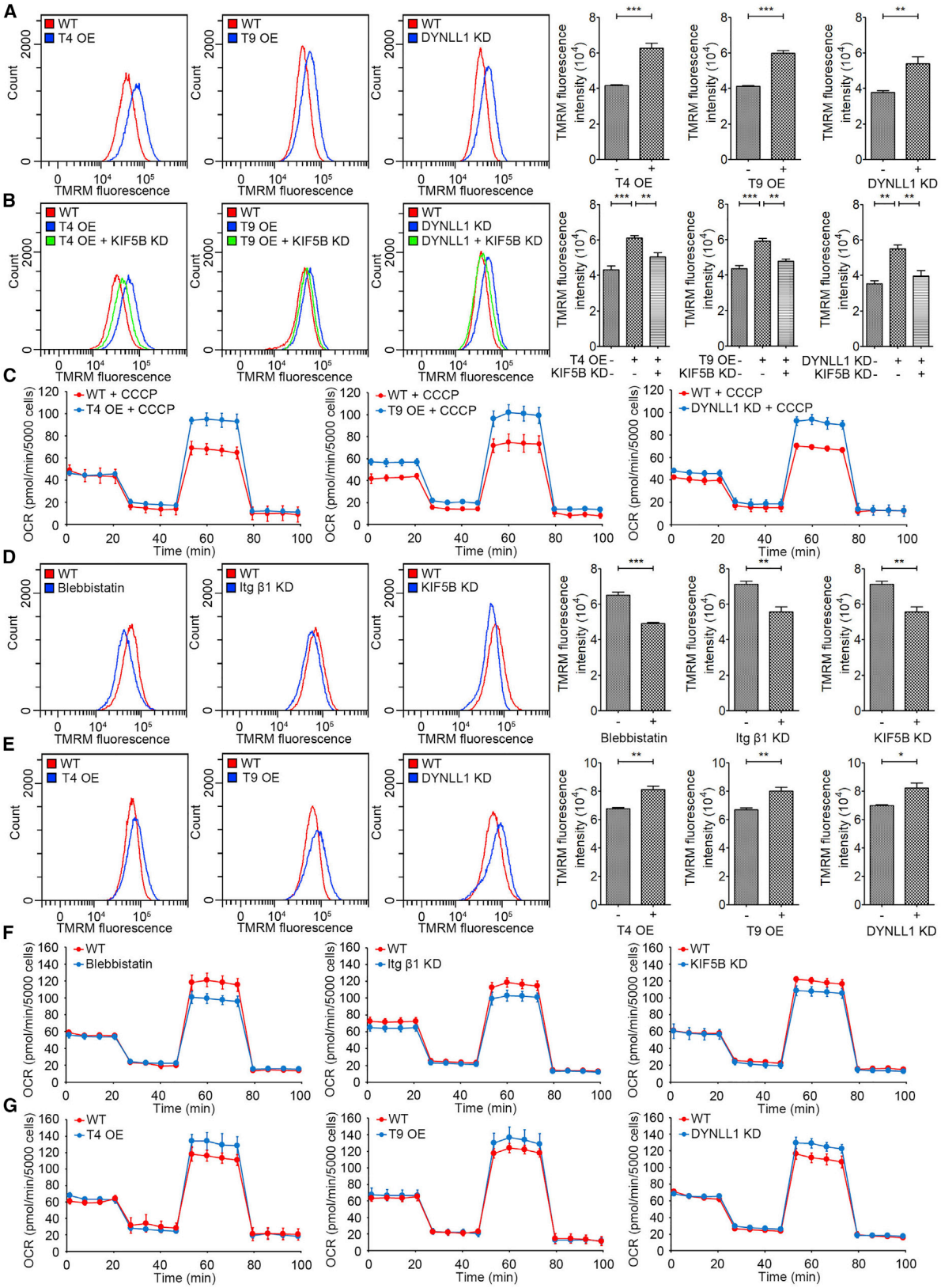

(legend on next page)

capacity (Figure 5F), while elevating mitocytosis enhances it (Figure 5G).

Mitocytosis maintains mitochondrial quality in macrophages during differentiation

Macrophages are capable of generating migrasomes and CCCP can trigger mitocytosis (Figures 1L, S5A, and S5B). We found that bone-marrow-derived macrophages (BMDMs) can form migrasomes on a glass surface without any coating but not on a surface that had undergone hydrophilic treatment (Figure 6A), which significantly reduced the migration of macrophages. Remarkably, simply culturing BMDMs on a hydrophilic surface caused significant loss of MMP, which suggests that migrasome formation is required for maintaining MMP in BMDMs (Figure 6B).

To further test the role of mitocytosis in BMDMs, we generated TSPAN9 knockout mice (Figure 6C). We isolated monocytes from WT and TSPAN9$^{-/-}$ mice and then differentiated them into BMDMs *ex vivo*. We found that the migrasome formation is markedly reduced in BMDMs derived from TSPAN9$^{-/-}$ mice (Figure 6D). Moreover, these BMDMs have significant loss of MMP compared to those from WT mice (Figures 6E).

To determine whether the loss of membrane potential is caused by mitocytosis or by a function of TSPAN9 independent of mitocytosis, we transfected TSPAN9$^{-/-}$ macrophages with TSPAN9 and then cultured these cells on an untreated surface or a hydrophilic surface. Expressing TSPAN9 partially restored the formation of migrasomes and MMP in cells grown on the untreated migrasome-forming surface but not in cells grown on the treated surface, which does not support migrasome formation (Figures 6F and 6G). Thus, TSPAN9 likely regulates MMPthrough mitocytosis.

To study the role of mitocytosis in a more physiologically relevant setting, we isolated peritoneal macrophages from WT and TSPAN9$^{-/-}$ mice. We found that the MMP is reduced in TSPAN9$^{-/-}$ peritoneal macrophages (Figure 7H). Interestingly, there was no difference in the MMP of immobile hepatocytes isolated from WT and TSPAN9$^{-/-}$, which indicates that knockout of TSPAN9 does not affect MMP in immobile cells (Figure 6I).

Mitocytosis maintains neutrophil mitochondrial quality *in vivo*

To investigate the physiological roles of mitocytosis *in vivo*, we choose neutrophils as our subject of study as they are highly migratory cells that are very abundant in the circulation. To label the neutrophils in mice, we injected PE-labeled anti-Ly-6G into the tail vein. We used one-photon spinning-disk microscopy to observe the liver and spleen. Although this imaging approach cannot observe deep into tissue, the blood vessels on the surface of tissues can nevertheless be very clearly observed.

We found that our *in vivo* staining approach labeled neutrophils efficiently. As shown in Figure 7A and Video S6, we found that migrasomes were extensively generated by circulating neutrophils. Next, we tested whether migrasomes generated by neutrophils contain mitochondria. We isolated the neutrophils and stained them with Mito-SOX to label damaged mitochondria and then we injected these neutrophils back into mice. We found that indeed many of the migrasomes generated by neutrophils contain Mito-SOX signal (Figure 7B). When we isolated migrasomes from blood, we found that around 87% of them originated from neutrophils (Figure 7C). We subjected the migrasomes to ultra-thin sectioning and examined them by TEM. The isolated migrasomes are highly homogeneous and share the morphological hallmarks of migrasomes. Importantly, many of the isolated migrasomes contain damaged mitochondria (Figure 7D). Accordingly, the isolated migrasomes contain various migrasomal and mitochondrial markers (Figure 7E). Thus, mitocytosis does occur *in vivo*.

Next, we investigate migrasome formation in TSPAN9$^{-/-}$ mice. To directly compare the rate of migrasome formation between WT and knockout neutrophils, we isolated neutrophils from WT and TSPAN9$^{-/-}$ mice and labeled them with different colors. We then injected the WT/TSPAN9$^{-/-}$ neutrophil mixture into WT mice (Figure 7F). As shown in Figures 7G and 7H and Video S7, we found that the formation of migrasomes by TSPAN9$^{-/-}$ neutrophils is significantly reduced.

To test whether reduced mitocytosis affects mitochondrial quality control, we isolated neutrophils from spleen and then measured their MMP. We found there are two populations of neutrophils, one with higher MMP, and the other with lower MMP. In the majority of WT mice, most neutrophils are in the higher MMP population. In contrast, in TSPAN9$^{-/-}$ mice, despite the considerable variation between different animals, the percentage of neutrophils with higher MMP is greatly reduced (Figure 7I).

To distinguish between the roles of TSPAN9 and migrasomes in mitochondrial quality control, we measured the MMP in mature neutrophils in bone marrow. Neutrophils are produced and matured in the bone marrow and then migrate into the circulation, where they undergo long-distance migration before reaching the spleen. We reasoned that, if migrasomes, but not TSPAN9, are required to maintain mitochondrial quality, there should be less difference between the MMP of WT and TSPAN9$^{-/-}$ bone-marrow neutrophils than between WT and

Figure 5. Mitocytosis protects cells from mitochondrial stress and maintains mitochondrial homeostasis

(A) MMP of WT, TSPAN4-expressing (T4 OE), TSPAN9-expressing (T9 OE), and DYNLL1-deficient (DYNLL1 KD) L929 cells. Quantification of TMRM fluorescence intensity is shown as the mean ± SEM. Data from three independent experiments were analyzed using two-tailed unpaired t tests (right panels).

(B) MMP of indicated L929 cells. Right panels, quantification of TMRM fluorescence intensity. Error bar, mean ± SEM. Experiments were independently repeated three times. Two-tailed unpaired t tests were used for statistical analyses.

(C) Oxygen consumption rate (OCR) of indicated cells. The graph represents the mean OCR ± SEM of three replicates.

(D) MMP of indicated L929 cell. The fluorescence intensity of TMRM was quantified as the mean ± SEM. Data from triplicated experiments were analyzed using two-tailed unpaired t tests (right panels).

(E) MMP of indicated cells. Right panels, quantification of TMRM fluorescence intensity. Error bar, ± SEM. Experiments were repeated three times. Two-tailed unpaired t tests were used for statistical analyses.

(F and G) OCR of indicated L929 cells. The graph represents the mean OCR ± SEM of three replicates.

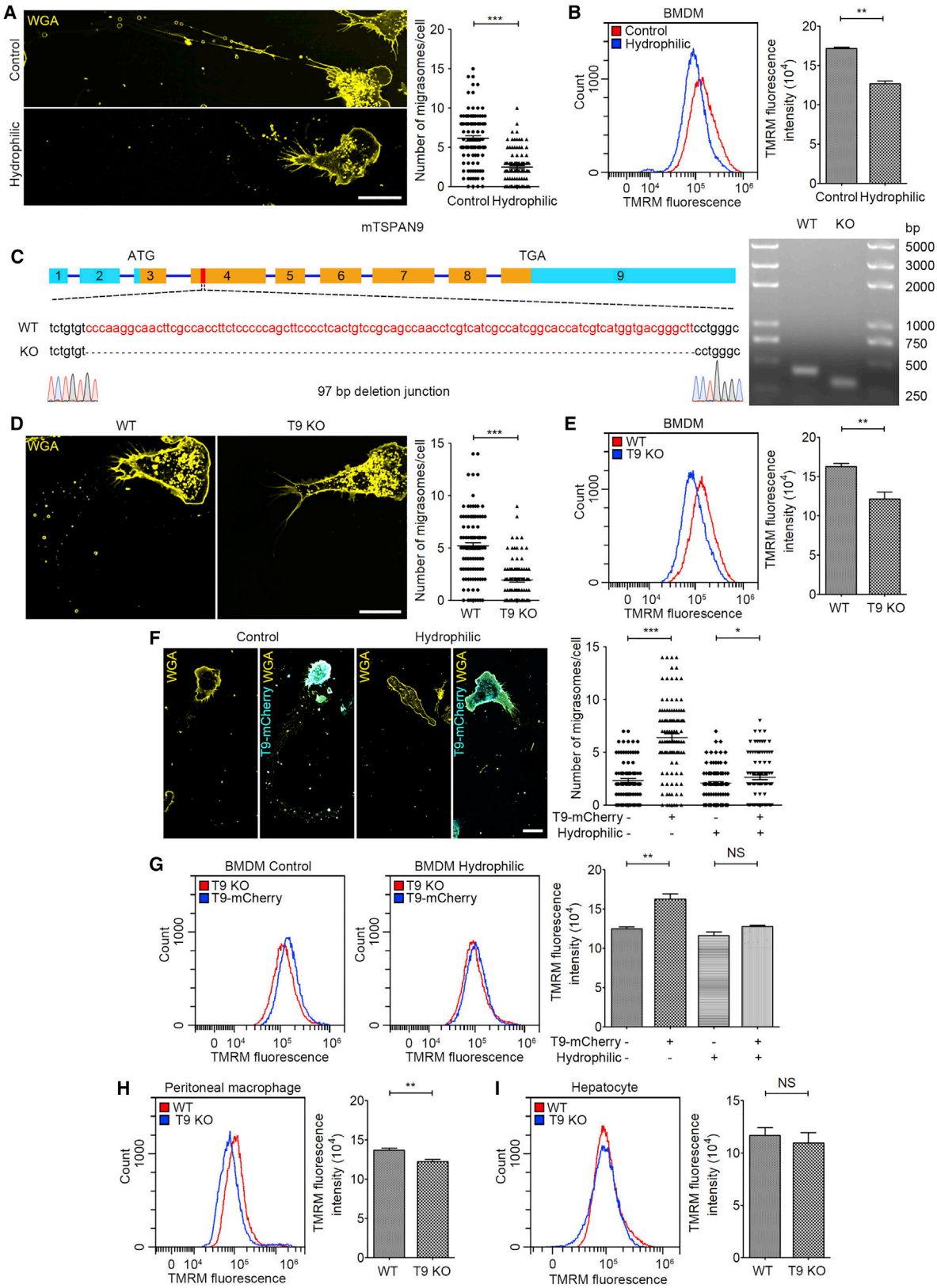

(legend on next page)

TSPAN9$^{-/-}$ spleen neutrophils. This is because bone-marrow neutrophils have not yet undergone their long-distance migration, and therefore mitocytosis has not yet kicked in. Indeed, we found there is almost no difference in MMP between WT and TSPAN9$^{-/-}$ bone-marrow neutrophils (Figure 7J). These data suggest that it is migrasomes, and not TSPAN9, that contribute to mitochondrial quality control.

Finally, we explored the physiological consequence of impaired mitocytosis in neutrophils. It is well established that accumulation of damaged mitochondria can impair the viability of cells. Thus, we measured the number of mature neutrophils in bone morrow and spleen of WT and TSPAN9$^{-/-}$ mice. We found that the number of neutrophils in bone marrow is very similar in both genotypes (Figure 7K), which indicates that the generation and maturation of neutrophils are normal in TSPAN9$^{-/-}$ mice. However, compared to WT mice, the number of neutrophils in spleen is reduced in TSPAN9$^{-/-}$ mice, which suggests that TSPAN9$^{-/-}$ neutrophils may have reduced viability (Figure 7L). To directly test the viability of neutrophils, we isolated bone-marrow neutrophils from WT and TSPAN9$^{-/-}$ mice and then labeled them with different doses of CFSE and injected equal numbers back into WT mice (Figure 7M). We found that after 1 day's circulation, WT neutrophils significantly outnumber TSPAN9$^{-/-}$ neutrophils (Figures 7M and 7N), which suggests that mitocytosis does contribute to the viability of neutrophils in the circulation.

DISCUSSION

Compared to stationary cells, migrating cells need to consume more energy to support migration, and thus they likely have a higher respiration rate, higher ROS generation, and a higher mitochondrial stress load. Therefore, migrating cells require additional mechanisms to mitigate this higher mitochondrial stress burden. It makes sense that mitocytosis, which is intrinsically associated with migration, is the mechanism of choice for mitochondrial quality control in migrating cells. In this sense, mitocytosis couples mitochondrial homeostasis with cell migration.

Mitocytosis is induced by mild mitochondrial stress. It is worth noting that 10 μM CCCP, which is the dose used to induce mitophagy, only marginally induces mitocytosis. This is probably explained by the fact that cells are barely migrating in the presence of 10 μM CCCP. We speculate that mitocytosis and mitophagy may serve as a two-gear system to maintain mitochondrial quality in migrating cells, with mitocytosis dealing with mild mitochondrial damage, which likely occurs frequently under physiological conditions, while mitophagy deals with severe mitochondrial damage related to pathological conditions.

The rate of mitocytosis is fairly low, which is not unexpected. Mitocytosis is a mitochondrial quality-control process for dealing with the very mild mitochondrial stress, which cells may encounter in physiological conditions. Thus, we do not expect that migrating cells will expel large amounts of mitochondria via mitocytosis. Damaged mitochondria release cytochrome C, which can trigger activation of the self-amplifying caspase cascade. Therefore, accumulation of even small numbers of damaged mitochondria may have a drastic effect in the long run. By continually removing damaged mitochondria, mitocytosis can help cells avoid the adverse effects associated with accumulation of dysfunctional mitochondria. This notion is supported by our data showing that cell viability and MMP are reduced in neutrophils with impaired migrasome formation.

In this study, we found that motor proteins such as KIF5B and dynein contribute to mitochondria quality control by playing key roles in regulating mitocytosis. It is worth noting that KIF5B and dynein may contribute to mitochondrial quality control through other mechanisms, as it has been reported that mitochondria can provide ROS to the leading edge of migrating cells, where ROS can regulate actin dynamics and be consumed during this process (Wang et al., 2011; Wilson and González-Billault, 2015). Mitochondrial dynamics is regulated by motor proteins, and ROS is an important source of mitochondrial toxicity. Thus, mitochondrial trafficking, which is mediated by motor proteins, may also contribute to the role of motor proteins in regulating mitochondrial quality control.

Limitations of study

We propose that mitocytosis is a mitochondrial quality-control process in migrating cells. At this point, at least 3 important questions remain. (1) We showed that mitocytosis maintains mitochondrial quality and viability in neutrophils. Our analysis is limited to mice in the steady state. Future studies using an

Figure 6. Mitocytosis maintains macrophage mitochondrial quality during differentiation

(A) BMDMs were cultured on confocal dishes with or without hydrophilic treatment for 12 h before visualization. Scale bar, 20 μm. Right panel, statistical analysis of the number of migrasomes per cell. Error bars, the mean ± SEM n > 100 cells from two independent experiments. Two-tailed unpaired t tests were used for statistical analyses.

(B) MMP of BMDMs plated on dish treated with indicated conditions. Quantification of TMRM fluorescence intensity is shown as the mean ± SEM. Data from two independent experiments were analyzed using two-tailed unpaired t tests (right panel).

(C) Schematic diagram of knockout site. Right panel, verification of the *Tspan9* KO mutation.

(D) Confocal images of WT and TSPAN9$^{-/-}$ BMDMs. Scale bar, 20 μm. The number of migrasomes per cell was quantified. Data were analyzed with two-tailed unpaired t tests, error bars, ± SEM n > 100 cells from three independent experiments (right panel).

(E) MMP of WT and TSPAN9$^{-/-}$ BMDMs. Right panel, quantification of TMRM fluorescence intensity. Error bar, ± SEM 3 repeats were done. Two-tailed unpaired t tests were used for statistical analyses.

(F) Confocal images of TSPAN9-mCherry expressing TSPAN9$^{-/-}$ BMDMs. Scale bar, 20 μm. Right panel, quantification of the number of migrasomes per cell. Error bars, ± SEM n > 100 cells from three independent experiments. Two-tailed unpaired t tests were used for statistical analyses.

(G) MMP of indicated BMDMs. Right panel, quantification of TMRM fluorescence intensity. Error bar, ± SEM 3 repeats were performed. Two-tailed unpaired t tests were used for statistical analyses.

(H and I) MMP of WT and TSPAN9$^{-/-}$ peritoneal macrophages (H) and hepatocytes (I). The fluorescence intensity of TMRM was quantified, error bar, ± SEM. Data from two independent experiments were analyzed using two-tailed unpaired t tests (right panel).

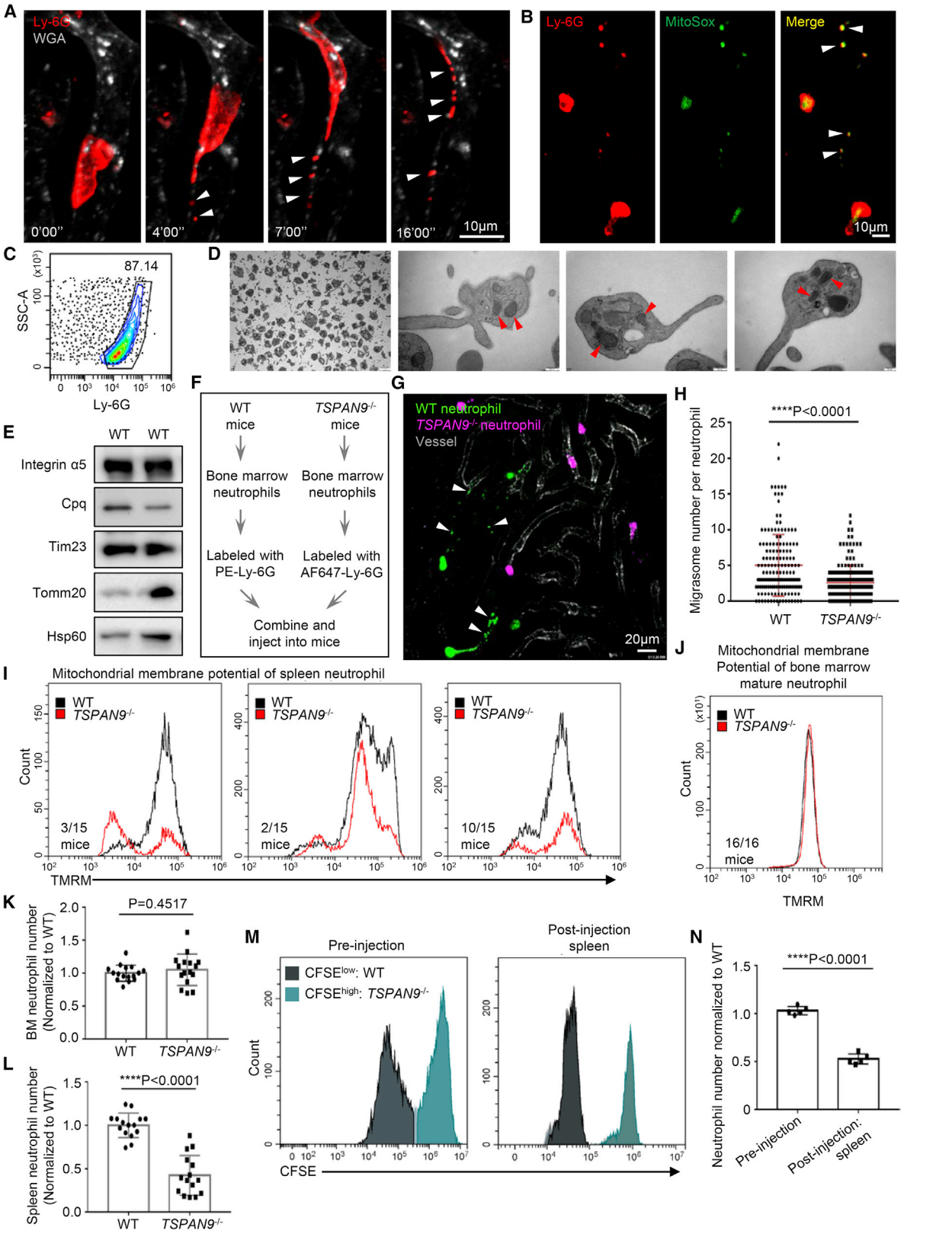

(legend on next page)

infection model are required to establish the role of mitocytosis in the immune response. In addition, the study should also be extended to other types of migratory immune cells. (2) We found that damaged mitochondria intrinsically avoid binding to the inward motor protein. However, the cues that signal the status of damaged mitochondria for mitocytosis still remain elusive. (3) It remains to be tested whether or not mitocytosis has other functions, for example, horizontal transfer of mitochondria between cells.

STAR★METHODS

Detailed methods are provided in the online version of this paper and include the following:

- KEY RESOURCES TABLE
- RESOURCE AVAILABILITY
  - Lead contact
  - Materials availability
  - Data and code availability
- EXPERIMENTAL MODEL AND SUBJECT DETAILS
  - Cells
  - Mice
- METHOD DETAILS
  - Cell transfection and virus infection
  - Isolation of migrasomes
  - Confocal imaging and image analysis
  - Transmission electron microscopy
  - Western blot
  - Mitochondrial fractionation
  - Preparation of S-100 cytosol from L929 cells
  - *In vitro* mitochondrial pull-down assay
  - Measurement of ROS
  - Measurement of mitochondrial membrane potential
  - Measurement of oxygen consumption rate
  - Intravital imaging
  - Migrasome purification from blood
  - Neutrophil viability analysis
  - Flow cytometry analysis
- QUANTIFICATION AND STATISTICAL ANALYSIS
  - Statistical analysis

SUPPLEMENTAL INFORMATION

Supplemental information can be found online at https://doi.org/10.1016/j.cell.2021.04.027.

ACKNOWLEDGMENTS

This research was supported by the National Natural Science Foundation of China (grant no. 92054301, 31790401, and 32030023), Beijing Municipal Science & Technology Commission (grant no. Z201100005320019), the Ministry of Science and Technology of the People's Republic of China (grant no. 2017YFA0503404 and 2016YFA0500202). We thank the State Key Laboratory of Membrane Biology, SLSTU-Nikon Biological Imaging Center, Core Facility, Center of Biomedical Analysis, Tsinghua University, for technical support. H.J. was funded by the Postdoctoral Program of Tsinghua University–Peking University Joint Center for Life Sciences. D.J. was supported by the Shuimu Tsinghua Scholar Program and Advanced Innovation Fellow program.

AUTHOR CONTRIBUTIONS

L.Y. conceived the experiments, L.Y. wrote the paper and supervised the project, and H.J. and D.J. carried out the experiments. X.H., X.L., and T.S. helped to purify migrasomes and construct plasmids. Y.L. and W.D. carried out the EM sample preparation and data acquisition, L.J. and Y.Y. helped to isolate macrophages, and X.W. helped to isolate primary hepatocytes. Y.-H.W. and Y.-H.W. provided mitochondrial heteroplasmic cells. X.H. contributed to the macrophage related experiments. All authors discussed the manuscript, commented on the project, and contributed to preparing the paper.

DECLARATION OF INTERESTS

The authors declare no competing interests.

Received: February 27, 2020
Revised: February 9, 2021
Accepted: April 16, 2021
Published: May 27, 2021

Figure 7. Mitocytosis maintains neutrophil mitochondrial quality *in vivo*

(A) Intravital imaging of mouse liver neutrophils. Labeled with anti-mouse Ly-6G (Gr-1) PE. AF647-WGA labels blood vessels. Scale bar, 10 μm. Arrowheads, migrasomes.

(B) Mito-SOX red-labeled neutrophils were injected back into liver blood vessels and imaged. Scale bar, 10 μm. Arrowheads, migrasomes.

(C) Flow-cytometry analysis of purified migrasomes.

(D) TEM images of purified migrasomes from mouse blood. Scale bar 2 μm. Enlarged images, 200 nm. Arrowheads, mitochondria.

(E) Western blot analysis of purified migrasomes from two mouse.

(F) Diagram of neutrophils imaging.

(G) Labeled WT and TSPAN9$^{-/-}$ neutrophils combined in equal amounts and injected back into WT mice and imaged. Scale bar, 20 μm. Arrowheads, migrasomes.

(H) Quantification of the number of migrasomes by WT and TSPAN9$^{-/-}$ neutrophils. Data were pooled from three independent experiments. WT, n = 166 cells, and TSPAN9$^{-/-}$, n = 177 cells. Data represent the mean ± SEM. Two-tailed unpaired t tests were used for statistical analyses.

(I and J) MMP analysis in neutrophils from spleen cell suspensions (I) and bone-marrow cell suspensions (J). Data were pooled from three independent experiments. For spleen, WT, n = 15 mice, and TSPAN9$^{-/-}$, n = 15 mice. For bone marrow, WT, n = 16 mice, and TSPAN9$^{-/-}$, n = 16 mice.

(K–L) Quantification of the number of neutrophils in bone marrow (K) and spleen (L). Data were pooled from more than three independent experiments. For spleen, WT, n = 15 mice, and TSPAN9$^{-/-}$, n = 15 mice. For bone marrow, WT, n = 16 mice, and TSPAN9$^{-/-}$, n = 16 mice. The mice are the same as those in (I) and (J). Data represent the mean ± SEM. Two-tailed unpaired t tests were used for statistical analyses.

(M) WT and TSPAN9$^{-/-}$ bone-marrow neutrophils were isolated and labeled with 0.5 μM CFSE (CFSE^{low}) and 5 μM CFSE (CFSE^{high}), respectively. The cells were combined in equal numbers and injected back into the tail vein of WT mice. After 16–24 h, CFSE^{low} and CFSE^{high} neutrophils were analyzed for cell viability.

(N) Quantification of the number of viable neutrophils, normalized to WT. n = 5 mice. Data represent the mean ± SEM. Experiments were independently repeated three times. Two-tailed unpaired t tests were used for statistical analyses.

REFERENCES

Davis, C.H., Kim, K.Y., Bushong, E.A., Mills, E.A., Boassa, D., Shih, T., Kinebuchi, M., Phan, S., Zhou, Y., Bihlmeyer, N.A., et al. (2014). Transcellular degradation of axonal mitochondria. Proc. Natl. Acad. Sci. USA *111*, 9633–9638.

Fernandes-Alnemri, T., Yu, J.W., Juliana, C., Solorzano, L., Kang, S., Wu, J., Datta, P., McCormick, M., Huang, L., McDermott, E., et al. (2010). The AIM2 inflammasome is critical for innate immunity to Francisella tularensis. Nat. Immunol. *11*, 385–393.

Hayakawa, K., Esposito, E., Wang, X., Terasaki, Y., Liu, Y., Xing, C., Ji, X., and Lo, E.H. (2016). Transfer of mitochondria from astrocytes to neurons after stroke. Nature *535*, 551–555.

Hoppins, S., and Nunnari, J. (2012). Cell Biology. Mitochondrial dynamics and apoptosis–the ER connection. Science *337*, 1052–1054.

Huang, Y., Zucker, B., Zhang, S., Elias, S., Zhu, Y., Chen, H., Ding, T., Li, Y., Sun, Y., Lou, J., et al. (2019). Migrasome formation is mediated by assembly of micron-scale tetraspanin macrodomains. Nat. Cell Biol. *21*, 991–1002.

Ji, L., Zhao, X., Zhang, B., Kang, L., Song, W., Zhao, B., Xie, W., Chen, L., and Hu, X. (2019). Slc6a8-Mediated Creatine Uptake and Accumulation Reprogram Macrophage Polarization via Regulating Cytokine Responses. Immunity *51*, 272–284.

Jiang, D., Jiang, Z., Lu, D., Wang, X., Liang, H., Zhang, J., Meng, Y., Li, Y., Wu, D., Huang, Y., et al. (2019). Migrasomes provide regional cues for organ morphogenesis during zebrafish gastrulation. Nat. Cell Biol. *21*, 966–977.

Jiao, H., Su, G.Q., Dong, W., Zhang, L., Xie, W., Yao, L.M., Chen, P., Wang, Z.X., Liou, Y.C., and You, H. (2015). Chaperone-like protein p32 regulates ULK1 stability and autophagy. Cell Death Differ. *22*, 1812–1823.

Liu, X., Kim, C.N., Yang, J., Jemmerson, R., and Wang, X. (1996). Induction of apoptotic program in cell-free extracts: requirement for dATP and cytochrome c. Cell *86*, 147–157.

Liu, C.Y., Lee, C.F., and Wei, Y.H. (2009). Activation of PKCdelta and ERK1/2 in the sensitivity to UV-induced apoptosis of human cells harboring 4977 bp deletion of mitochondrial DNA. Biochim. Biophys. Acta *1792*, 783–790.

Ma, L., Li, Y., Peng, J., Wu, D., Zhao, X., Cui, Y., Chen, L., Yan, X., Du, Y., and Yu, L. (2015). Discovery of the migrasome, an organelle mediating release of cytoplasmic contents during cell migration. Cell Res. *25*, 24–38.

MacDonald, G., Shi, L., Vande Velde, C., Lieberman, J., and Greenberg, A.H. (1999). Mitochondria-dependent and -independent regulation of Granzyme B-induced apoptosis. J. Exp. Med. *189*, 131–144.

Melentijevic, I., Toth, M.L., Arnold, M.L., Guasp, R.J., Harinath, G., Nguyen, K.C., Taub, D., Parker, J.A., Neri, C., Gabel, C.V., et al. (2017). C. elegans neurons jettison protein aggregates and mitochondria under neurotoxic stress. Nature *542*, 367–371.

Pickles, S., Vigié, P., and Youle, R.J. (2018). Mitophagy and Quality Control Mechanisms in Mitochondrial Maintenance. Curr. Biol. *28*, R170–R185.

Porteous, W.K., James, A.M., Sheard, P.W., Porteous, C.M., Packer, M.A., Hyslop, S.J., Melton, J.V., Pang, C.Y., Wei, Y.H., and Murphy, M.P. (1998). Bioenergetic consequences of accumulating the common 4977-bp mitochondrial DNA deletion. Eur. J. Biochem. *257*, 192–201.

Quintero, O.A., DiVito, M.M., Adikes, R.C., Kortan, M.B., Case, L.B., Lier, A.J., Panaretos, N.S., Slater, S.Q., Rengarajan, M., Feliu, M., and Cheney, R.E. (2009). Human Myo19 is a novel myosin that associates with mitochondria. Curr. Biol. *19*, 2008–2013.

Sheng, Z.H. (2014). Mitochondrial trafficking and anchoring in neurons: New insight and implications. J. Cell Biol. *204*, 1087–1098.

Shneyer, B.I., Ušaj, M., and Henn, A. (2016). Myo19 is an outer mitochondrial membrane motor and effector of starvation-induced filopodia. J. Cell Sci. *129*, 543–556.

Shneyer, B.I., Usaj, M., Wiesel-Motiuk, N., Regev, R., and Henn, A. (2017). ROS induced distribution of mitochondria to filopodia by Myo19 depends on a class specific tryptophan in the motor domain. Sci Rep. *7*, 11577.

Tanaka, Y., Kanai, Y., Okada, Y., Nonaka, S., Takeda, S., Harada, A., and Hirokawa, N. (1998). Targeted disruption of mouse conventional kinesin heavy chain, kif5B, results in abnormal perinuclear clustering of mitochondria. Cell *93*, 1147–1158.

Torralba, D., Baixauli, F., and Sánchez-Madrid, F. (2016). Mitochondria Know No Boundaries: Mechanisms and Functions of Intercellular Mitochondrial Transfer. Front. Cell Dev. Biol. *4*, 107.

Wang, Y., Zang, Q.S., Liu, Z., Wu, Q., Maass, D., Dulan, G., Shaul, P.W., Melito, L., Frantz, D.E., Kilgore, J.A., et al. (2011). Regulation of VEGF-induced endothelial cell migration by mitochondrial reactive oxygen species. Am. J. Physiol. Cell Physiol. *301*, C695–C704.

Wei, Y.H., Lee, C.F., Lee, H.C., Ma, Y.S., Wang, C.W., Lu, C.Y., and Pang, C.Y. (2001). Increases of mitochondrial mass and mitochondrial genome in association with enhanced oxidative stress in human cells harboring 4,977 BP-deleted mitochondrial DNA. Ann. N Y Acad. Sci. *928*, 97–112.

Wilson, C., and González-Billault, C. (2015). Regulation of cytoskeletal dynamics by redox signaling and oxidative stress: implications for neuronal development and trafficking. Front. Cell. Neurosci. *9*, 381.

Wu, D., Xu, Y., Ding, T., Zu, Y., Yang, C., and Yu, L. (2017). Pairing of integrins with ECM proteins determines migrasome formation. Cell Res. *27*, 1397–1400.

Youle, R.J. (2019). Mitochondria—Striking a balance between host and endosymbiont. Science *365*, eaaw9855.

Youle, R.J., and van der Bliek, A.M. (2012). Mitochondrial fission, fusion, and stress. Science *337*, 1062–1065.

STAR★METHODS

KEY RESOURCES TABLE

REAGENT OR RESOURCE	SOURCE	IDENTIFIER
Antibodies		
Anti-TOM20	Abcam	Cat# ab186735: RRID:AB_2889972
Anti-HSP60	Abcam	Cat# ab46798: RRID:AB_881444
Anti-KIF5B	Abcam	Cat# ab167429; RRID:AB_2715530
Anti-Drp1	Abcam	Cat# ab184247
Anti-DYNLL1	Abcam	Cat# ab51603; RRID:AB_2093654
Anti-MYO19	Abcam	Cat# ab174286
Anti-MYO19	Abcam	Cat# ab155219
Anti-Integrin α5	Cell Signaling Technology	Cat# 4705; RRID:AB_2233962
Anti-Integrin β1	Cell Signaling Technology	Cat# 4706; RRID:AB_823544
Anti-Atg5	Cell Signaling Technology	Cat# 12994; RRID:AB_2630393
Anti-TIM23	BD Biosciences	Cat# 611222; RRID:AB_398754
Anti-GAPDH	Proteintech Group	Cat# 60004-1-Ig; RRID:AB_2107436
Anti-MFN1	Proteintech Group	Cat# 13798-1-AP; RRID:AB_2266318
Anti-MFN2	Proteintech Group	Cat# 12186-1-AP; RRID:AB_2266320
Anti-GFP	Roche	Cat# 11814460001; RRID:AB_390913
Anti-DsRed	Clontech	Cat# 632496; RRID:AB_10013483
Anti-CPQ antibody	Sigma-Aldrich	Cat# HPA023235-100UL; RRID:AB_1855257
Anti-Ly-6G/Ly-6C-PE (RB6-8C5)	eBioscience	Cat# 12-5931-82; RRID:AB_466045
Anti-mouse F4/80-APC	BioLegend	Cat# 123116; RRID:AB_893481
Anti-mouse Ly-6G-Alexa Fluor 647	BioLegend	Cat# 127610; RRID:AB_1134159
Anti-mouse/human CD11b-PerCP/Cyanine5.5 a	BioLegend	Cat# 101227; RRID:AB_893233
Goat Anti-Rabbit IgG (H+L)	Jackson	Cat# 111-035-003; RRID:AB_2313567
Goat Anti-Mouse IgG (H+L)	Jackson	Cat# 115-035-003; RRID:AB_10015289
Chemicals, peptides, and recombinant proteins		
Fibronectin	ThermoFisher	Cat# PHE0023
Wheat Germ Agglutinin (WGA)	ThermoFisher	Cat# W7024
Antimycin A	Abcam	Cat# ab141904
Oligomycin	Abcam	Cat# ab141829
CCCP	BestBio	Cat# BB-4177
TMRM	BestBio	Cat# BB-41054
JC-1	BestBio	Cat# BB-4105
Blebbistatin	Abcam	Cat# ab120425
DFP	Sigma-Aldrich	Cat# Y0001976
MitoSOX Red mitochondrial superoxide indicator	ThermoFisher	Cat# M36008
MitoTracker Red CM-H2XRos	ThermoFisher	Cat# M7513
Proteinase K	Sigma-Aldrich	Cat# P8811
Vigofect	Vigorous	Cat# T001
Anti-Ly6G MicroBeads Ultrapure, mouse	Miltenyi Biotec	Cat# 130-120-337
CFSE	BestBio	Cat# BB-4211-500T
G418	Amresco	Cat# E859
Hygromycin B	Roche	Cat# 10843555001
Puromycin	ThermoFisher	Cat# A1113803

(*Continued on next page*)

Continued

REAGENT OR RESOURCE	SOURCE	IDENTIFIER
Critical commercial assays		
BCA Protein Assay Kit	Pierce	Cat# 23227
ClonExpress II One Step Cloning Kit	Vazyme	Cat# C112-01
EasyPure PCR Purification Kit	TransGen Biotech	Cat# EP101-01
Universal DNA Purification Kit	TIANGEN	Cat# DP214-03
TIANamp Genomic DNA Kit	TIANGEN	Cat# DP304-02
EndoFree Mini Plasmid Kit	TIANGEN	Cat# DP118-02
Lysosome Isolation Kit	Sigma-Aldrich	Cat# LYSISO1
XF cell mito stress test kit	Seahorse Bioscience	Cat# 103015-100
RevertAid First Strand cDNA Synthesis Kit	ThermoFisher	Cat# K1622
Zombie NIR Fixable Viability Kit	Biolegend	Cat# 423105
QuadroMACS Separator	Miltenyi Biotec	Cat# 130-091-051
Experimental models: cell lines		
L929 cell	Xiaoyu Hu Laboratory	ATCC Number: CCL-1
NRK cell	ATCC	ATCC Number: CRL-6509
MiaCaPa-2 cell	Yupei Zhao Laboratory	ATCC Number: CRL-1420
HUVEC	Xiaoli Tian Laboratory	N/A
BMDM	This paper	N/A
Mitochondrial heteroplasmic cell	Yau-Huei Wei Laboratory	N/A
Experimental models: organisms/strains		
Mouse: C57BL/6J	Animal facility at Tsinghua University	N/A
Mouse: Tspan9−/−	This paper	N/A
Recombinant DNA		
Plasmid: MitoDsRed in pB-CAG-BGH	This paper	N/A
Plasmid: TSPAN4-mCherry in pB-CAG-BGH	This paper	N/A
Plasmid: TSPAN4-GFP in pB-CAG-BGH	This paper	N/A
Plasmid: TOM20-GFP in pB-CAG-BGH	This paper	N/A
Plasmid: TOM20-BFP in pB-CAG-BGH	This paper	N/A
Plasmid: GFP-Myo19-WT in pB-CAG-BGH	This paper	N/A
Plasmid: GFP-Myo19-W140V in pB-CAG-BGH	This paper	N/A
Plasmid: KIF5B-GFP in pB-CAG-BGH	This paper	N/A
Plasmid: mCherry-DYNLL1 in pB-CAG-BGH	This paper	N/A
Plasmid: TSPAN9-mCherry in plvx-puro	This paper	N/A
Plasmid: mtKeima in pB-CAG-BGH	This paper	N/A
Software and algorithms		
Imaris software	Bitplane AG	https://imaris.oxinst.com
ImageJ	NIH Image for the Macintosh	https://imagej.nih.gov/ij/index.html
GraphPad Prism 5 (or 7)	GraphPad Software	https://www.graphpad.com/
CytExpert software	Beckman Coulter	https://www.advanceduninstaller.com/CytExpert-2e59738422f3e7c7f4dd76136917715f-application.htm
NIS-Elements analysis 5.0 software	Nikon	https://www.microscope.healthcare.nikon.com/products/software/nis-elements/nis-elements-advanced-research
Seahorse XFe-96 software	Seahorse Bioscience	https://www.agilent.com/en/products/cell-analysis/software-download-for-wave-desktop
Fusion	Andor technology	https://andor.oxinst.com/products/dragonfly

RESOURCE AVAILABILITY

Lead contact

Further information and requests for resources and reagents should be directed to and will be fulfilled by the Lead Contact, Li Yu (liyulab@mail.tsinghua.edu.cn).

Materials availability

This study did not generate new unique reagents. Plasmids generated in this study will be made available on request by the Lead Contact.

Data and code availability

No unpublished custom code, software, algorithm or sequencing data were generated in this study.

EXPERIMENTAL MODEL AND SUBJECT DETAILS

Cells

L929, NRK and MiaCaPa-2 cells were cultured in DMEM (Hyclone) medium supplemented with 10% FBS (Biological Industries), 2 mM GlutaMAX and 100 U/ml penicillin-streptomycin in 5% CO_2 at 37°C. HUVEC cells were grown in ECM (ScienCell) supplemented with 20% FBS, 1% ECGS and 100 U/ml penicillin-streptomycin.

Mouse bone marrow-derived macrophages (BMDMs) were obtained from WT or TSPAN9−/− C57BL/6 mice as previously described (Fernandes-Alnemri et al., 2010). Monocytes and BMDMs were maintained in L929 conditioned medium (DMEM supplemented with 10% FBS, 10% L929 supernatant and 100 U/ml penicillin-streptomycin) for 5 days. Suspension cells were discarded and adherent BMDMs were used in the following experiments.

Peritoneal macrophages were acquired from WT or TSPAN9−/− C57BL/6 mice as described previously (Ji et al., 2019). Mice were injected intraperitoneally with 1.0 mL of 4% sterile thioglycollate. After 4 days, thioglycollate-elicited macrophages were isolated from peritoneum by lavage using 5 mL PBS. Peritoneal macrophages stained with APC anti-mouse F4/80 Antibody (BioLegend) were analyzed by flow cytometry.

The heteroplasmic cells harboring 20% wild-type mtDNA and 80% mtDNA with a 4977-bp deletion of the ETC genes were made by fusing mtDNA-less (ρ0) human 143B osteosarcoma cells with denucleated skin fibroblasts (Liu et al., 2009). The cells were grown in DMEM supplemented with 5% FBS, 100 μg/ml pyruvate, 50 μg/ml uridine, 200 U/ml penicillin G, 200 μg/ml streptomycin sulfate and 0.5 μg/ml amphotericin B at 37°C.

Neutrophil isolation was performed using Anti-Ly-6G MicroBeads UltraPure (Miltenyi Biotec, 130-120-337). Bone marrow cell suspensions were isolated and treated with Ammonium-Chloride-Potassium (ACK) lysis buffer for 2 min to lyse red blood cells. The mixture of bone marrow cells was then incubated with Anti-Ly-6G MicroBeads for 20 min at 4°C. Cells were resuspended with PBS (containing 2% FBS) and subjected to positive selection through LS Columns (Miltenyi Biotec, 130-042-401) on a QuadroMACS Separator (Miltenyi Biotec, 130-091-051). The columns were disconnected from the separator, and the neutrophils were washed out with 5 mL PBS (containing 2% FBS).

Mice

We used CRISPR/Cas9 to knock out *Tspan9* in C57BL/6 mice. The sgRNA sequence used for CRISPR/Cas9 was 5′-GAAGGTGGC-GAAGTTGCCTT-3′. Gender- and age-matched WT C57BL/6 mice were used as controls for TSPAN9−/− animals. Mice were housed in individually ventilated cages in a temperature- and light-regulated room in specific pathogen-free (SPF) conditions and received food and water *ad libitum*. All animal procedures and experiments were performed following the guidelines of the Laboratory Animal Research Center of Tsinghua University. Protocols for mouse experiments were approved by the Institutional Animal Care and Use Committee of Tsinghua University. The laboratory animal facility has been licensed by the Science and Technology Commission of Beijing Municipality (SYXK-2014-0024) and accredited by the Association for Assessment and Accreditation of Laboratory Animal Care International.

METHOD DETAILS

Cell transfection and virus infection

Vigofect was used for cell transfection according to the manufacturer's manual. Cells were seeded in a 35 mm dish and grown to 80% confluency, and then transfected with 200 μL NaCl (150 mM) that contained 2 μL Vigofect and 5 μg plasmid. The transfection mix was replaced with fresh medium after 4-6 hr. Cells were cultured for another 20 hr for protein expression.

Lentiviral production and infection were conducted as previously described (Jiao et al., 2015) and the manufacturer's instructions (MISSION Lentiviral Packaging Mix). Briefly, lentivirus was produced from 293T cells transfected with lentiviral vectors using the above Vigofect transfection protocol. For virus infection, cells were seeded in a 35 mm dish at 50%–60% density. Growth medium was removed and virus-containing polybrene (8 μg/ml) was added to cells. After 24 hours, cells were selected in fresh medium

containing 5 μg/ml puromycin until drug-resistant colonies became visible. pLKO.1-puro vectors bearing shRNA were used for knockdown, and plvx-puro vectors encoding TSPAN9-mCherry were used for rescue in TSPAN9 KO BMDMs. shRNA sequences were as follows: mouse KIF5B: 5′-CCTATGTTCCTTATCGAGATA-3′, mouse DYNLL1: 5′-GCTTAGTATCTTTGTGCTCAA-3′, mouse Drp1: 5′-GCTTCAGATCAGAGAACTTAT-3′, mouse MFN1: 5′-GCGTTTAAGCAGCAGTTTGTA-3′, mouse MFN2: 5′-GCTACAGCTCATCATCAGTTA-3′, mouse DYNLL1: 5′-GCCCATATCAAGAAGGAGTTT-3′, mouse Itgβ1: 5′-GCACGATGTGATGATTTAGAA-3′.

The PiggyBac Transposon Vector System was used to generate the L929 stably expressing cell lines. L929 cells were co-transfected with pB (transposon vector) and pBASE (transposase vector) at a ratio of 1:3. After 24 hr, the cells were selected in medium containing 600 μg/ml G418 or 200 μg/ml hygromycin B for 3-5 days, followed by single cell sorting with a fluorescence activated cell sorting. These single cell clones were further identified using confocal microscopy.

Isolation of migrasomes

Migrasome isolation was performed by iodixanol-sucrose density gradient centrifugation using an Optiprep kit (Sigma-Aldrich, LYSISO1), and the procedure was based on a modification of previous protocols (Ma et al., 2015). Briefly, cells were grown in 150 mm dishes precoated with fibronectin (1 μg/ml) in full DMEM medium for 12 hr. Growth medium was disposed of and cells were washed to remove other extracellular vesicles in the medium. Cells were trypsinized and collected in 50 mL tubes. All subsequent manipulations were performed at 4°C. Cells and large debris were removed by centrifugation at 1000 g for 10 min followed by 4000 g for 20 min. Crude migrasomes were then collected as the pellet by centrifugation at 18,000 g for 30 min. Migrasome fractionation was performed by density gradient centrifugation, using Optiprep as the density medium. The crude migrasome sample was prepared by first resuspending the pellet with 400 μl 1 × extraction buffer mixed with 400 μl 10% Optiprep. First, a step gradient was built starting with 50% (500 μl), followed by 40% (500 μl), 35% (500 μl), 30% (500 μl), 25% (500 μl), 20% (500 μl), 15% (500 μl), 10% (500 μl), 5% (500 μl) and crude migrasomes (5%, 800 μl). Second, the prepared gradient was centrifuged at 150,000 g for 4 hr at 4°C in an MLS-50 rotor (Beckman). Third, samples were collected from top to bottom (500 μl per fraction). Each fraction was mixed with the same volume of PBS (500 μl) and centrifuged at 18,000 g for 30 min to collect the pellet. The pellets were washed with PBS and centrifuged again at 18,000 g for 30 min. The samples were compatible with western blot analysis, TEM, cryo-EM and mass spectrometry.

Confocal imaging and image analysis

35 mm confocal dishes were precoated with fibronectin (10 μg/ml) at 37°C for 1 hour. Cells were cultured in fibronectin-precoated confocal dishes for 10-12 hr. Confocal snapshot images were acquired using a NIKON A1RSiHD25 laser scanning confocal microscope at 1024 × 1024 pixels. For live-cell imaging, cells were cultured in fibronectin-precoated confocal dishes for 4-6 hours before imaging. Cells were maintained at 37°C with 5% CO_2, and monitored with a NIKON A1 microscope at 1024 × 1024 pixels. Images were processed with ImageJ and Imaris software 8.1.4, and statistical analyses were conducted using Graphpad Prism 5. For presentation, final images were deconvoluted by NIS-Elements analysis 5.0 software.

Transmission electron microscopy

Cells were grown in 35 mm dishes precoated with fibronectin (10 μg/ml). After 10-12 hours, cells were pre-fixed using a 1:1 ratio of growth medium to 2.5% glutaraldehyde for 5 min at room temperature. Cells were further fixed with 2.5% glutaraldehyde in PB buffer for 2 hours at room temperature, washed three times with PBS and dehydrated in an ascending gradual series of ethanol (50%, 70%, 90%, 95%, and 100%) for 8 min each. Samples were infiltrated with and embedded in SPON12 resin. After polymerizing for 48 h at 60°C, 70-nm-thick ultrathin sections were cut using a diamond knife, and then picked up with Formvar-coated copper grids (100 mesh). The sections were double stained with uranyl acetate and lead citrate. After air drying, samples were examined with a transmission electron microscope H-7650B at an acceleration voltage of 80 kV.

Western blot

Cells or migrasomes were lysed by SDS lysis buffer (2.5% in PBS), then boiled for 10-20 min at 95°C. Equal amounts of protein were separated on SDS-PAGE gels of an appropriate percentage according to the MW of target proteins, followed by electrophoretic transfer onto PVDF membranes. Membranes were blocked with 5% non-fat milk in TBST buffer, and incubated with primary antibody in solution 1 (TOYOBO) overnight at 4°C. Membranes were incubated with HRP-conjugated secondary antibody for 1 hr at room temperature, and signals were detected with a WESTAR ηC 2.0 kit (CYANAGEN).

The following primary antibodies were used for western blot analyses at the indicated dilution: anti-TOM20 (1:5000), anti-TIM23 (1:5000), anti-HSP60 (1:5000), anti-GAPDH (1:5000), anti-Integrin α5 (1:1000), anti-KIF5B (1:5000), anti-Drp1 (1:2000), anti-MFN1 (1:1000), anti-MFN2 (1:1000) anti-DYNLL1 (1:5000), anti-MYO19 (1:1000) and anti-Integrin β1 (1:1000).

Mitochondrial fractionation

Mitochondrial fractionation was performed following published protocols with minor modifications (Tanaka et al., 1998). Briefly, cells were washed with PBS several times, suspended and broken in H-S buffer (10 mM HEPES, pH 7.4, 320 mM sucrose, 5 mM $MgSO_4$, 1 mM EGTA, 1 mM DTT, and protease inhibitors) by passing 15 times through 1 mL syringes fitted with 27G needles. After centrifugation at 1000 × g for 10 min at 4°C, the supernatant was further centrifuged at 11 400 × g for 20 min at 4°C to precipitate the crude mitochondrial fraction. The pellet was resuspended in H-S buffer and subjected to sucrose gradient centrifugation. First, the

centrifuge tube was layered with a HEPES-buffered sucrose step density gradient (0.3 mL of 2.3 M, 1.7 mL of 1.7 M, and 1.5 mL of 1 M). Then, the crude mitochondrial fraction was layered on the top of the sucrose gradient. The gradient was centrifuged at 100 000 × g for 30 min at 4°C, and the mitochondria accumulated at the interface of the 1 M and 1.7 M sucrose layers. 500 μL of the 1 M/1.7 M interface was recovered, diluted 3-fold with H-S buffer, and pelleted by centrifuging for 10 min at 11 400 × g. This wash step was repeated 3 times.

Preparation of S-100 cytosol from L929 cells

The S-100 cytosol fraction was prepared as described previously with some modifications (Liu et al., 1996). Briefly, cells were washed with ice-cold PBS, resuspended in ice-cold buffer S (20 mM HEPES, pH 7.4, 10 mM KCl, 1.5 mM $MgCl_2$, 1 mM EDTA, 1 mM EGTA, 1 mM DTT, and protease inhibitors). After sitting on ice for 15 min, the cells were lysed by 15 passes through 1 mL syringes fitted with 27G needles. The homogenate was centrifuged at 1000 × g for 10 min at 4°C to pellet the nuclei, and the supernatant was further centrifuged at 100,000 × g for 60 min at 4°C. The resulting supernatant (S-100 cytosol) was used for the *in vitro* cell-free system assay.

In vitro mitochondrial pull-down assay

Mitochondrial fractions and S-100 cytosolic fractions were obtained as described above from L929 cells. The *in vitro* mitochondrial pull-down assay was performed according to established protocols with some modifications (MacDonald et al., 1999). Briefly, 100 μL diluted mitochondria (500 μg/ml) were mixed with 1 mL L929 S-100 cytosol in dilution buffer (20 mM HEPES, pH 7.4, 2 mM $MgCl_2$ and 1 mM DTT) for 4 hr at 37°C. After incubation, the reaction mixture was centrifuged to pellet the mitochondria, and the purified mitochondria were washed three times and then run on SDS-PAGE gels followed by western blotting with the indicated antibodies.

Measurement of ROS

Mitochondrial ROS production was measured using MitoSOX probe according to the manufacturer's protocol (Life Technologies). In brief, cells were cultured in fibronectin-precoated confocal dishes and treated as described. Cells were gently washed once with PBS and then were incubated with 3 μM MitoSOX Red and 1 μg/ml WGA in HBSS for 10 min at 37°C. After three gentle washes with warm PBS, cells were cultured in HBSS and subjected to confocal analysis.

Measurement of mitochondrial membrane potential

TMRM and JC-1 were used to determine mitochondrial membrane potential according to the manufacturer's manual. Briefly, after treatment as described, cells were gently washed once with warm PBS. Cells were incubated in either TMRM or JC-1 working solution for 20 min at 37°C, and then gently washed three times with warm PBS. For flow cytometry assay, cells were trypsin-digested and suspended in HBSS. The TMRM intensity in different groups was measured by FACS (Beckman Coulter CytoFLEX LX) and analyzed using CytExpert software. Data were obtained from three independent experiments, and 50,000 cells were examined per group in each experiment. For microscopy assay, cells stained with WGA were immersed in HBSS and then imaged as quickly as possible. Confocal images were acquired using a NIKON A1 microscope.

Measurement of oxygen consumption rate

Oxygen consumption rates of cells were measured with the Seahorse XF^e96 Extracellular Flux Analyzer (Seahorse Bioscience) according to manufacturer's instructions. In brief, after treatment as described, 5000 cells (per well) were cultured in FN-precoated XF^e96 well plates with medium for 12 hr. Before measurement, cell medium was replaced by XF assay medium (XF Base Medium supplemented with 25 mM glucose, 1 mM pyruvate, 6 mM L-glutamine and adjusted to pH 7.4). Cells were then maintained in 175 μL/well of XF assay medium at 37°C in an incubator without supplied CO_2 for 1 hour. During the incubation time, 16 μM oligomycin (8 ×), 18 μM FCCP (9 ×), 10 μM rotenone (10 ×) and 10 μM antimycin A (10 ×) in XF assay medium were successively loaded into the injection ports in the XF^e96 sensor cartridge. The assay procedure was set as 'Mix-03:00, Wait-00:00, Measurement-03:00' for 4 cycles. After measurement, cells were digested with trypsin and counted for cell number. Oxygen consumption rates of cells were normalized to cell number. Datasets were analyzed by Wave software (Agilent Technologies).

Intravital imaging

For neutrophil imaging, 5 mg of AF647-WGA (Thermo Fisher, W32466) and 1 μg of PE-Ly-6G/Ly-6C antibody (eBioscience, 12-5931-82) were injected into C57BL6/J mice (male, 8-12 weeks) by intravenous injection (i.v.). After 5 min, anesthesia was induced in the mice by intraperitoneal injection (i.p.) of Avertin (375 mg/kg). Subsequently, the mice were dissected to expose the liver on a plate with a round cover glass in the center for spinning-disk confocal microscopy imaging.

For Mito-SOX staining imaging, neutrophils were isolated from bone marrow of C57BL6/J mice and stained with Mito-SOX red (1:400) and AF647-Ly-6G antibody (BioLegend, 127610, 1:200) at 37°C for 30 min. Neutrophils were washed and injected into the spleen of anesthetized mice. Subsequently, the mice were dissected to expose the liver on a plate with a round cover glass in the center for spinning-disk confocal microscopy imaging.

For WT and TSPAN9−/− neutrophil imaging, neutrophils were isolated from WT and TSPAN9−/− mice, and then stained with PE-Ly-6G/Ly-6C antibody and AF647-Ly-6G antibody, respectively. Equal numbers of neutrophils were washed with PBS and combined

together for injection into the spleen of C57BL6/J mice which had been injected (i.v.) with 5 mg AF647-WGA to label vessels. Subsequently, the mice were anesthetized and dissected to expose the liver on a plate with a round cover glass in the center for spinning-disk confocal microscopy imaging.

Migrasome purification from blood

Anesthesia was induced in the mice by Avertin injection (375 mg/kg, i.p.), and blood was collected from the ocular venous plexus and put into a tube containing blood collection buffer (PBS+10 mM EDTA) on ice. The blood mixture was then centrifuged at 1000 g, 4°C for 5 min, followed by 2000 g, 4°C for 15 min to remove the blood cells and finally at 20000 g, 4°C for 40 min. The pellet is the crude migrasome fraction.

Neutrophil viability analysis

Bone marrow neutrophils were isolated from WT and TSPAN9−/− mice, and labeled with 0.5 μM CFSE ($CFSE^{low}$) (BestBio, BB-4211-500T) and 5 μM CFSE ($CFSE^{high}$) respectively. WT and TSPAN9−/− neutrophils were then combined together in equal numbers and injected back into the tail vein of C57BL6/J mice. After 16-24 hours, spleen cell suspensions were isolated and treated with ACK buffer to lyse the red blood cells. Red blood cell-free spleen cells were stained with a Zombie NIR Fixable Viability Kit (BioLegend, 423105) and subjected to flow cytometry analysis. Viable cells were gated on the $CFSE^{low}$ and $CFSE^{high}$ populations and analyzed for cell number.

Flow cytometry analysis

Spleen cell suspensions and/or bone marrow cell suspensions were isolated and treated with ACK buffer to lyse the red blood cells. Red blood cell-free spleen cells or bone marrow cells were stained with AF647 anti-mouse Ly-6G (1:200), PerCP/Cyanine5.5 anti-CD11b (1:200) and TMRM for 15 min at 4°C, and then subjected to flow cytometry analysis with a Beckman Coulter CytoFLEX LX. Viable cells were gated on the Ly-6G+/CD11b+ population and analyzed for TMRM intensity and/or cell numbers.

QUANTIFICATION AND STATISTICAL ANALYSIS

Statistical analysis

Statistical parameters and significance are reported in the Figures and the Figure Legends. Statistical analyses were conducted using the unpaired two-tailed t test in Graphpad Prism 5 (or 7) software (GraphPad Software). Error bars are the mean ± SEM. Significance is indicated by asterisks: *$p < 0.05$, **$p < 0.01$, ***$p < 0.001$, ****$p < 0.0001$, NS, not significant.

Supplemental figures

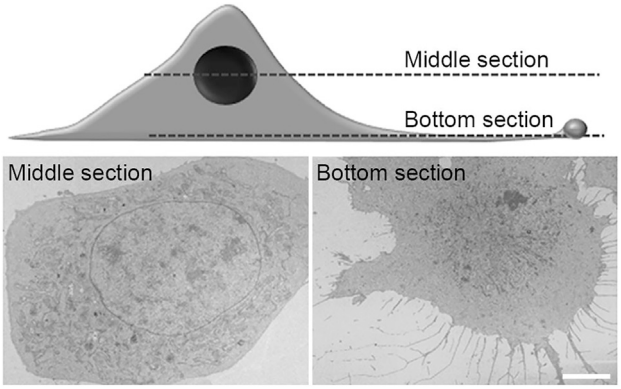

Figure S1. TEM analysis of bottom and middle sections of cells, related to Figure 2

Top: diagram of the location of ultra-thin sections. Bottom: representative TEM micrographs of L929 cells sectioned through the middle layer and the bottom layer. Scale bar, 10 μm.

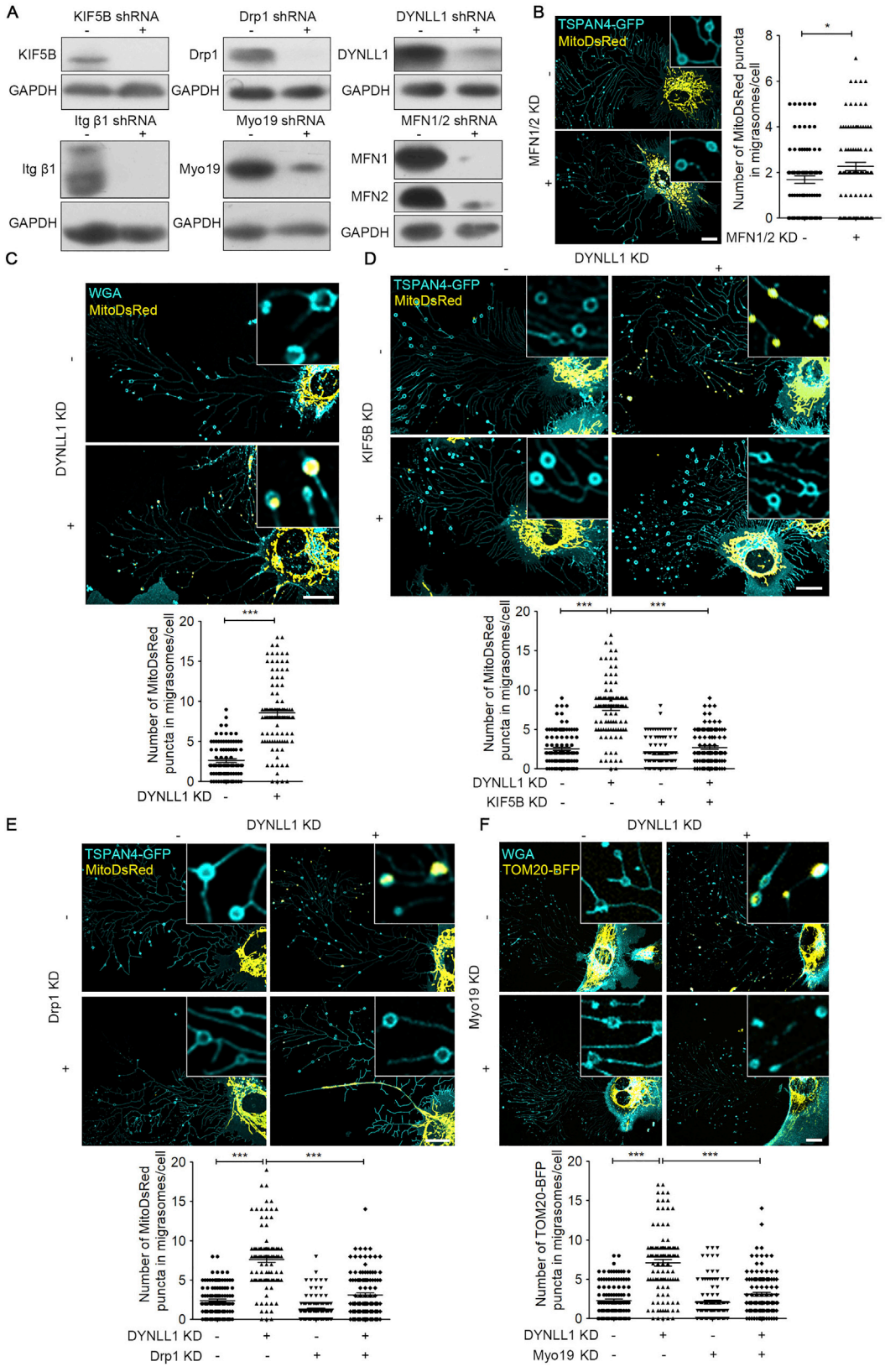

(legend on next page)

Figure S2. Dynein knockdown promotes mitocytosis in untreated cells, related to Figure 2

(A) Detection of shRNA knockdown efficiency.

(B) L929 cells stably expressing TSPAN4-GFP and MitoDsRed were infected with NS or MFN1/MFN2-shRNA lentiviruses. Cells were cultured on FN-coated confocal dishes and then subjected to confocal analysis. Scale bar, 20 μm. The right panel shows statistical analysis of the number of MitoDsRed puncta in migrasomes per cell. The error bars represent the mean ± SEM n > 100 cells from three independent experiments. Two-tailed unpaired t tests were used for statistical analyses.

(C) MitoDsRed-expressing L929 cells infected with lentiviral NS or DYNLL1-shRNA were stained with WGA and analyzed with a NIKON A1 confocal microscope. Scale bar, 20 μm. The lower panel shows statistical analysis of the number of MitoDsRed puncta in migrasomes per cell. The error bars represent the mean ± SEM n > 100 cells from three independent experiments. Two-tailed unpaired t tests were used for statistical analyses.

(D) L929 cells stably expressing TSPAN4-GFP and MitoDsRed were infected with lentivirus encoding the indicated shRNAs. Cells were cultured on FN-coated confocal dishes and analyzed with a NIKON A1 confocal microscope. Scale bar, 20 μm. Quantification of the number of MitoDsRed puncta in migrasomes per cell is shown as the mean ± SEM for triplicate samples of > 100 cells. Two-tailed unpaired t tests were used for statistical analyses (lower panel).

(E) L929 cells stably expressing TSPAN4-GFP and MitoDsRed were infected with the indicated lentiviral shRNA constructs. Cells were seeded into confocal dishes and visualized with a NIKON A1 confocal microscope. Scale bar, 20 μm. The number of MitoDsRed puncta in migrasomes per cell was quantified. Data are presented as mean ± SEM n > 100 cells from three independent experiments. Two-tailed unpaired t tests were used for statistical analyses (lower panel).

(F) L929-TOM20-BFP cells infected with the indicated lentiviral vectors were stained with WGA and subjected to confocal analysis. Scale bar, 20 μm. The lower panel shows statistical analysis of the number of TOM20-BFP puncta in migrasomes per cell. The error bars are the mean ± SEM n > 100 cells from three independent experiments. Two-tailed unpaired t tests were used for statistical analyses.

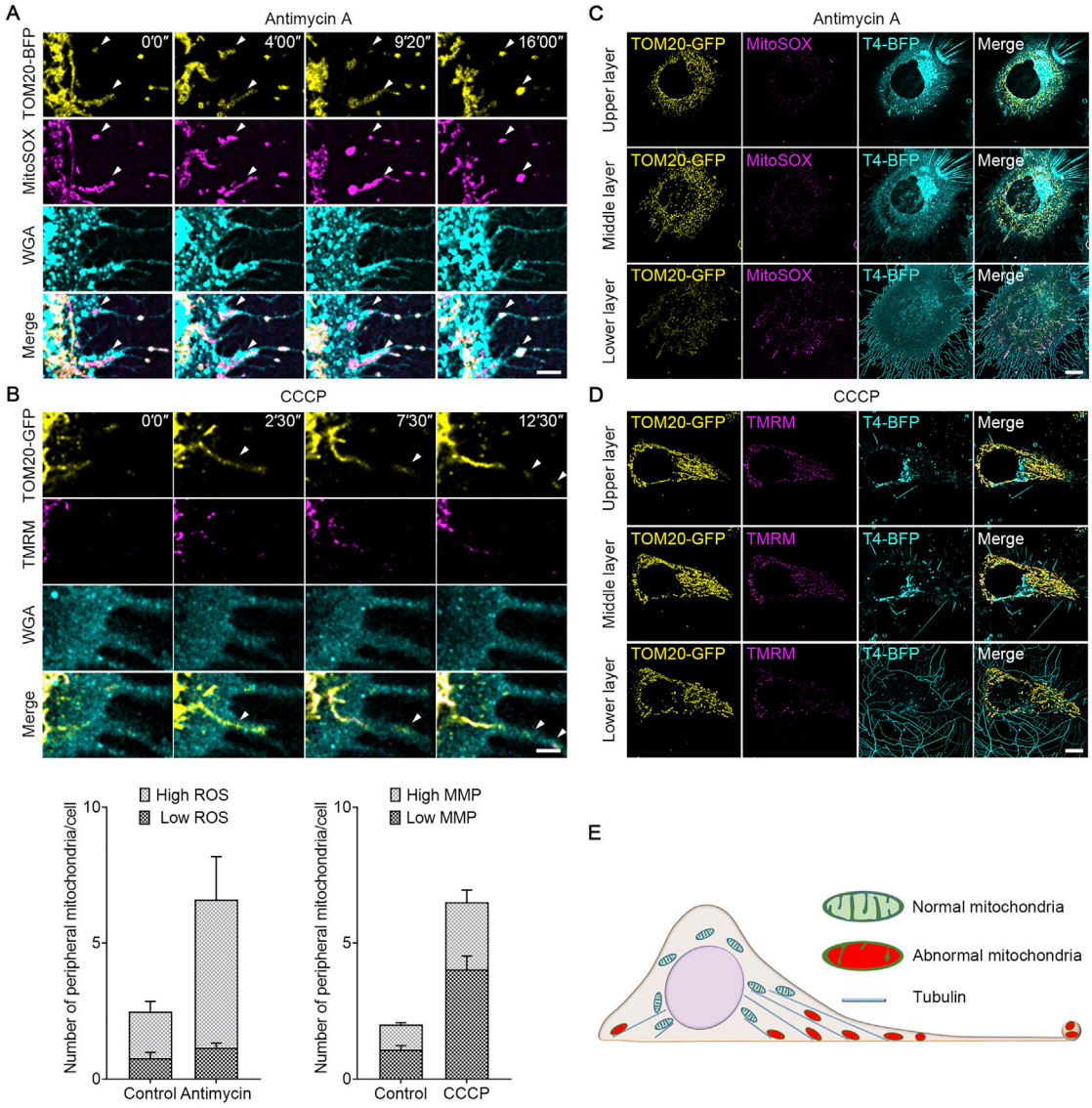

Figure S3. Damaged mitochondria are transported to the cell periphery before disposal by mitocytosis, related to Figure 3

(A) L929-TOM20-BFP cells were treated with or without 2 μM Antimycin A and stained with WGA and MitoSOX. Cells were then subjected to time-lapse imaging using a NIKON A1 confocal microscope. Time interval, 80 s. Scale bar, 5 μm. The lower panel shows quantification of the number of peripheral mitochondria with low ROS or high ROS per cell. n > 30 cells from three independent experiments. Two-tailed unpaired t tests were used for statistical analyses.

(B) L929-TOM20-GFP cells, either untreated or treated with 2 μM CCCP, were stained with WGA and TMRM followed by time-lapse imaging analysis. Time interval, 150 s. Scale bar, 5 μm. The lower panel shows quantification of the number of peripheral mitochondria with low MMP or high MMP per cell. n > 30 cells from three independent experiments. Two-tailed unpaired t tests were used for statistical analyses.

(C) L929 cells stably expressing TSPAN4-BFP and TOM20-GFP were treated with 2 μM Antimycin A and stained with MitoSOX. Cells were then subjected to z stack imaging using a NIKON A1 confocal microscope. Scale bar, 10 μm.

(D) L929 cells stably expressing TSPAN4-BFP and TOM20-GFP, treated with 2 μM CCCP, were stained with TMRM followed by z stack imaging analysis. Scale bar, 10 μm.

(E) Schematic diagram illustrating how damaged mitochondria are transported to the bottom layer of the cell.

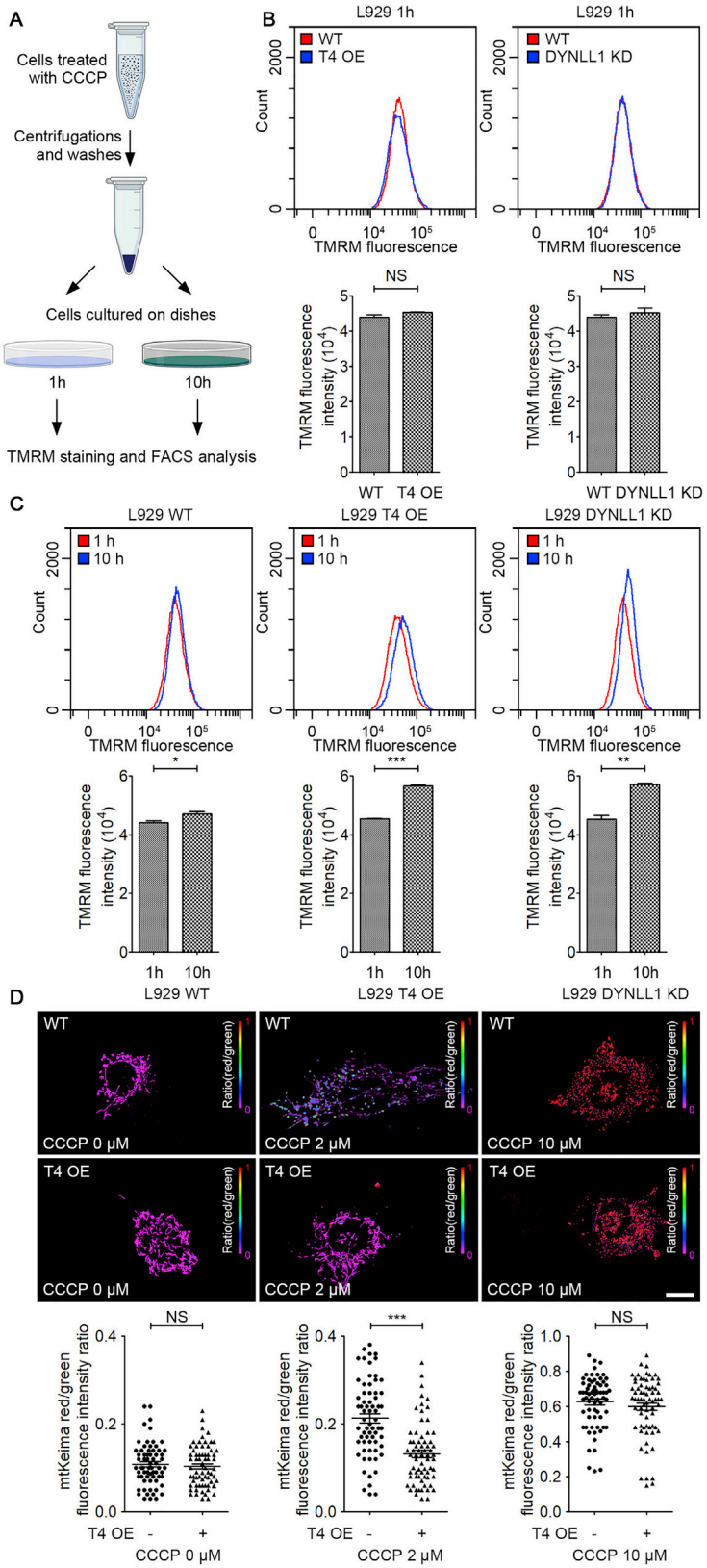

(legend on next page)

Figure S4. Mitocytosis can mitigate mitochondrial damage induced by mild mitochondrial stress, related to Figure 5

(A-C) WT, TSPAN4-expressing and DYNLL1-deficient L929 cells were pre-treated with 2 μM CCCP for 1 hr. Cells were then cultured on FN-coated dishes for the indicated time. Mitochondrial membrane potential was detected by FACS analysis of TMRM-stained cells. TMRM fluorescence intensity was quantified and shown as the the mean ± SEM. Experiments were independently repeated three times. Two-tailed unpaired t tests were used for statistical analyses.

(D) L929 cells stably expressing mtKeima were cultured on fibronectin (FN)-coated confocal dishes for 2 hr, and then treated with the indicated concentrations of CCCP for 20 hr. The cells were imaged with 488 nm (green) or 561 nm (red) light excitation with a NIKON A1 confocal microscope. Scale bar, 20 μm. Mitophagy is observed as an increased red/green fluorescence ratio. The lower panels show statistical analysis of the mtKeima red/green fluorescence intensity ratio. Data are presented as mean ± SEM n > 50 cells from three independent experiments. Two-tailed unpaired t tests were used for statistical analyses.

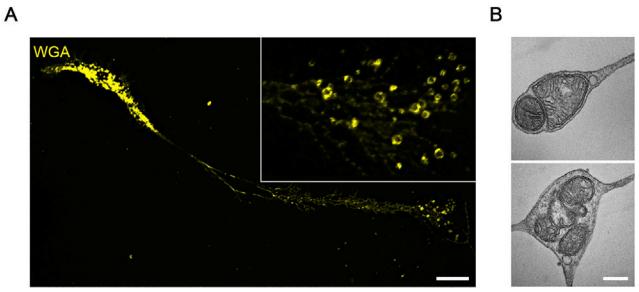

Figure S5. Mitocytosis occurs in macrophages, related to Figure 6

(A) Representative confocal images of mouse bone marrow-derived macrophages (BMDMs). BMDMs were cultured on confocal dishes for 12 hr. Cells were then stained with WGA before analysis with a NIKON A1 confocal microscope. Scale bar, 20 μm.

(B) BMDMs were grown on the glass surface of a 35 mm dish for 12 hr. Representative TEM images of enlarged migrasomes containing mitochondria are shown. Scale bar, 200 nm.